HHS Public Access

Author manuscript

*Neuron*. Author manuscript; available in PMC 2023 January 05.

Published in final edited form as:

*Neuron*. 2022 January 05; 110(1): 120–138.e4. doi:10.1016/j.neuron.2021.10.005.

# Visual Thalamocortical Mechanisms of Waking State Dependent Activity and Alpha Oscillations

**Dennis B. Nestvogel**[1,*], **David A. McCormick**[1,2,*]

[1]Institute of Neuroscience, University of Oregon, Eugene, Oregon, 97403, USA

[2]Lead Contact

## Summary:

The brain exhibits distinct patterns of recurrent activity closely related to the behavioral state. The neural mechanisms that underlie state-dependent activity in the awake animal are incompletely understood. Here, we demonstrate that two types of state-dependent activity - rapid arousal/movement related signals and a 3–5 Hz alpha-like rhythm - in the primary visual cortex (V1) of mice strongly correlate with activity in the visual thalamus. Inactivation of V1 does not interrupt arousal/movement signals in most visual thalamic neurons, but it abolishes the 3–5 Hz oscillation. Silencing of the visual thalamus similarly eradicates the alpha-like rhythm and perturbs arousal/movement-related activation in V1. Intracellular recordings in thalamic neurons reveal the 3–5 Hz oscillation to be associated with rhythmic low threshold $Ca^{2+}$ spikes. Our results indicate that thalamocortical interactions through ionotropic signaling, together with cell-intrinsic properties of thalamocortical cells, play a crucial role in shaping state-dependent activity in V1 of the awake animal.

## eTOC blurb

The authors performed intra- and extracellular recordings in the visual thalamus and visual cortex of mice to reveal a crucial role of thalamocortical interactions in shaping movement/arousal related signals in visual cortex and in regulating a 3–5 Hz oscillation thought to be an evolutionary precursor to the primate alpha rhythm.

### Keywords

Brain State; Alpha Oscillation; Primary Visual Cortex; Thalamus; Arousal; Movement

[*]Correspondence: dennisnestvogel@gmail.com (D.B.N.), davidmc@uoregon.edu (D.A.M.).

Author Contributions

D.B.N. and D.A.M. conceived and designed the study. D.B.N. performed experiments and data analysis. D.B.N. and D.A.M. wrote the paper.

Declaration of Interests

The authors declare no competing interests.

## Introduction

Spontaneous, ongoing activity in the waking brain is highly variable and can be classified according to distinct states and rhythms. These brain states are strongly related to animal behavior such as movements and the level of arousal and appear to be one of the strongest determinants of neural activity across the neocortex (Dolensek et al., 2020; McGinley et al., 2015a; Musall et al., 2019; Nath et al., 2019; Niell and Stryker, 2010; Poulet and Petersen, 2008; Reimer et al., 2014; Salkoff et al., 2020; Schneider et al., 2014; Stringer et al., 2019).

One example of a distinct state in the awake brain is the alpha-rhythm (8–12 Hz) first described by Hans Berger in the late 1920s in the human visual cortex (Berger, 1929). Alpha rhythms are particularly strong during states of mental relaxation and eye closure, although a few studies have also reported increases associated with attention and stimulus presentation (Schmid et al., 2012). The cellular and network mechanisms by which alpha oscillations are generated in the visual system are incompletely understood. Studies suggest that the alpha rhythm may primarily originate in the neocortex in layer 2,3 (Halgren et al., 2019), or layer 5 (Silva et al., 1991). Other evidence indicates that visual thalamic nuclei, such as the pulvinar/lateral posterior nucleus (LP) (Saalmann et al. 2012), and/or the dorsolateral geniculate nucleus (dLGN) (Hughes and Crunelli, 2005) are the primary drivers of the visual cortical alpha waves, with high threshold spike bursting proposed as a cell intrinsic mechanism (Crunelli et al., 2018; Hughes and Crunelli, 2005; Hughes et al., 2004; Lorincz et al., 2009). In mice, a state-dependent 3–5 Hz rhythm shares features of the primate alpha rhythm and has been proposed to be an evolutionary precursor (Einstein, 2017; Senzai et al., 2019). The neural mechanism of the mouse 3–5 Hz rhythm is currently unknown.

Another example of a distinct brain state in mouse V1 is the strong suppression of delta (0.5–4 Hz), and increase of gamma (30–60 Hz) power in the local field potential (LFP) during high arousal levels (i.e. large pupil diameters) and/or locomotion, which is associated with an increase in the amplitude of visually evoked responses (Niell and Stryker, 2010; Polack et al., 2013; Reimer et al., 2014). On the level of the membrane potential of excitatory V1 neurons, the transition from stillness to locomotion/high arousal is associated with a change from slowly fluctuating synaptic activity to a steady depolarization (Bennett et al., 2013; Polack et al., 2013; Reimer et al., 2014). Several studies have addressed the neural mechanisms underlying this increase in gamma activity and sensory gain in V1 and have suggested the involvement of neuromodulatory pathways (e.g. noradrenergic and cholinergic) (Fu et al., 2014; Lee et al., 2014; Leinweber et al., 2017; Pinto et al., 2013; Polack et al., 2013), changes in the activity of intracortical inhibitory networks (Fu et al., 2014; Polack et al., 2013; Reimer et al., 2014), and feedback from secondary motor cortex (Leinweber et al., 2017). These different neural pathways work through kinetically different mechanisms (e.g. metabotropic vs. ionotropic receptors) and understanding these kinetics more fully would narrow the possible underlying mechanisms. Indeed, it is not yet fully known if the mechanisms of cortical activation that are associated with movement results from the activation of movement-related structures, or whether this brain activation represents arousal that is concomitant with movement (McGinley et al., 2015b; Petty et al. 2020).

A possible significant contribution of subcortical structures to state-dependent waking V1 network dynamics has recently been suggested based upon the ability of locomotion to alter the activity of early visual brain structures, such as the retina (Liang et al., 2020; Schröder et al., 2020), the dorsolateral geniculate nucleus (dLGN) ( Aydın et al., 2018; Erisken et al., 2014; Roth et al., 2016), the lateral posterior nucleus (LP; mouse equivalent of the pulvinar) (Roth et al., 2016; Blot et al., 2021) and the superior colliculus (SC) (Ito et al., 2017; Savier et al., 2019; Schröder et al., 2020). Interestingly, studies in the mouse primary somatosensory cortex (S1) have shown that thalamic activity is necessary for the steady depolarization associated with whisker movement (Eggermann et al., 2014; Poulet et al., 2012), but it is not known whether this reflects a conserved mechanism that broadly applies to arousal/movement related brain state changes in other sensory systems.

By using intra- and extracellular recording techniques in awake behaving mice together with pharmacological and optogenetic manipulations, we studied the role of thalamocortical interactions in generating the state-dependent alpha-like oscillation and for regulating brain state changes associated with arousal and movements (facial and limb) in mouse V1. Our results indicate that the alpha-like oscillation in mice reflects a thalamocortical rhythm that involves low threshold $Ca^{2+}$ spike (LTS) mediated action potential (AP) bursting in thalamic neurons, depends upon thalamocortical interactions, and predominantly occurs during reduction in movement and arousal. Furthermore, we found that visual thalamic activity correlates strongly with rapid arousal/movement-related signals in V1 and appears to profoundly shape these signals in V1. Finally, we observed similar rapid state changes during spontaneous periods of increased arousal (pupil dilation) without overt movement, suggesting that a significant component of these rapid transitions in state-dependent activity may operate independently of movement.

## Results

To study the role of thalamic signaling in regulating state-dependent changes in V1, we measured postsynaptic potentials in layer 2,3 neurons through whole-cell recordings in awake head-fixed mice, while monitoring locomotion (wheel movements), whisker movements (whisker pad motion energy), and changes in pupil area (Fig. 1A–D). Whisker pad motion energy is a sensitive and informative indicator of the global movement state, with no movement in the whisker pad associated with complete or near complete behavioral quiescence (e.g. Supplemental movie 1). Recent studies employing $Ca^{2+}$-imaging and extracellular electrophysiology recordings reported a strong relationship between spontaneous cortical activity and whisker pad movements (Musall et al., 2019; Salkoff et al., 2020; Stringer et al., 2019). The exact timing and kinetics of whisker associated signals in V1 have not been studied and we speculated that addressing this issue would yield important insights into the mechanism that underlies these signals. Tight coupling within the range of tens of milliseconds or less between the onset of whisker movements and the occurrence of postsynaptic signals, as well as fast rise times, would support the hypothesis that whisker movement associated state changes in V1 are mediated via ionotropic signaling. Such fast signaling, in turn, could originate from structures such as the thalamus (Poulet et al., 2012).

To study the timing and kinetics of whisker associated signals in V1, we monitored the face of the mouse at a rate of 8 msec/frame (125 Hz; see Star Methods). By relating spontaneous behavior to membrane potential changes, we observed several recurring and identifiable states (Fig. 1 and Supplementary Movie 1): 1) behavioral quiescence with small pupil diameter, typically associated with the strong presence of lower frequency (<4 Hz) oscillations in synaptic activity (Fig.1E, slow oscil. shown in green); 2) whisker movements with and without locomotion, associated with rapid and sustained depolarization (Fig. 1E,F, sust.depol. shown in red); 3) cessation, or strong reduction, of motor movements, correlated with a 3–5 Hz oscillation (Fig 1E, 3–5 Hz oscil. shown in blue). Closer inspection of these 3–5 Hz oscillations revealed that they were associated with rhythmic barrages of synaptic activity arriving in V1 neurons (Fig. 1G). Finally, on rare occasions, we observed pupil dilations without overt wheel/whisker movements (see below; Fig. S1A–C), Supplementary Movie 1).

Since the prevalence of slow oscillatory activity during behavioral quiescence has been studied extensively previously (McCormick et al., 2020), we did not examine it further here. Instead, we sought to test the hypothesis that thalamocortical interactions may be responsible for both the rapid depolarization of cortical neurons during arousal and/or movement, as well as the generation of the 3–5 Hz alpha-like rhythm.

## Changes in visual cortical synaptic dynamics associated with whisker movement exhibit rapid kinetics

We recorded from a total of 52 layer 2/3 (L2,3) V1 neurons in 41 mice to study whisker movement/arousal associated membrane potential changes. The physiological features of these cells suggested that they were excitatory neurons (Fig. S2) (McCormick et al., 1985). As in the cell illustrated in Fig.1C–G, we generally observed that the onset of whisking was associated with a rapid depolarization. These rapid depolarizations occurred even in the absence of visible light, supporting the notion that they reflect genuine brain state changes as opposed to originating from sensory input at the retina (Fig. S3). In accordance with previous results on locomotion and pupil dilations (Bennett et al., 2013; Polack et al., 2013; Reimer et al., 2014), we found that the membrane potential was less variable during whisker movement (which may also include locomotion) (median quiet 13.67 $mV^2$ [19.49–9.85 IQR]); median whisking 12.67 [17.27 – 8.08 IQR]; paired t-test, p = 0.001; Fig. S2H) and AP firing was significantly increased on average (median quiet 0.36 spks/s [1.08–0.11 IQR].; median whisking 0.54 spks/s [1.59–0.08 IQR]; Wilcoxon signed rank sum test, p = 0.008) (Fig. S2A).

Rapid and sustained depolarizations appeared to be more closely coupled, in time, to movement of the whiskers rather than locomotion (which is less frequent than whisker movements), and pupil dilations (which exhibit slow temporal kinetics; Fig. 1 and Fig. S2M,N). Specifically, the grand average membrane potential depolarization response occurred nearly simultaneously with the onset of whisker movements (Fig. 1H) with a median half maximum time of 86.09 ms [111.0–30.18 IQR] (Fig. S2N) and a 20%−80% rise time of 158.31 ms [276.93–105.9 IQR] (Fig. S2M). We found that membrane potential depolarization responses were more loosely coupled to locomotion onsets with a half

maximum time of −49.68 ms [−45.74-(−172.8) IQR] (Wilcoxon rank sum test, $p < 0.001$) (Fig. S2N) and a 20%−80% rise time of 283.24 ms [416.03–163.23 IQR] (Wilcoxon rank sum test, $p = 0.001$) (Fig. S2M). Whisker movement typically preceded the onset of locomotion and we speculate that jitter in the onset of whisk bouts in comparison to locomotion onset contributed to the slower averaged rise time when depolarizations were sorted according to locomotion onset (Fig. 1I). Both whisker movement and locomotion were associated with pupil dilations and these pupil dilations were less tightly coupled to the visual cortical depolarizations than movements, presumably resulting in part from the slower kinetics of pupillary changes (Fig. 1H,I; Fig. S1C).

On rare occasions, we observed pupil dilations in the apparent absence of whisker movement or locomotion (Fig. S1A–C, supplementary movie 1). We studied this phenomenon in greater detail by visually screening the 52 recordings of the L2/3 cells and detected a total of 131 instances in 35 recordings (Fig. S1C). Interestingly, these rare instances of arousal without overt movement were also associated with rapid depolarization of visual cortical neurons, indicating that overt movement per se is not required for this phenomenon to occur.

What are the neural mechanisms that underlie the rapid state changes in V1? Our results of the fast rise times and tight coupling of movement related cortical membrane potential depolarizations support the hypothesis that fast ionotropic signaling underlies these changes, as opposed to slow metabotropic signaling. Previous studies have shown that the thalamus plays a crucial role in regulating whisker movement-related depolarization in S1 (Poulet et al., 2012), but it is not known whether the visual thalamus plays an important role for whisker movement related state-changes in V1. Extracellular recordings have revealed a fraction of dLGN neurons to exhibit increased activity during locomotion (Erisken et al., 2014; Roth et al., 2016). Movement signals have also been reported in LP visual thalamic neurons (Petty et al., 2020; Roth et al., 2016). However, the kinetics of these state changes are not fully known. To address this question, we performed intracellular recordings in excitatory layer 2,3 V1 neurons in combination with high-density Neuropixels probe extracellular recordings in the two major visual thalamic nuclei (dLGN and LP) (Fig. 2). In addition, we performed in-vivo whole-cell recordings in these two structures to study the timing of membrane potential depolarizations associated with movements (Fig. 3), similar to the experiments described above for L2/3 V1 neurons.

Results from these experiments revealed that membrane potential depolarizations in L2/3 V1 neurons associated with whisker movement were accompanied by increased AP firing in dLGN and LP neurons (Fig. 2A–F). Further analysis revealed that the median AP firing rate was significantly higher in visual thalamic neurons during whisking when compared to quiet periods (Fig. 2G–H). Our intracellular recordings from neurons in the LP and dLGN (n = 6 LP cells, n = 2 dLGN cells) (Figs. 3A–D) similarly revealed increased AP firing during whisker movement in visual thalamic neurons (median quiet 5.26 spks/s [9.45–2.98 IQR]); median whisk 7.97 spks/s [13.56–5.71 IQR], $p = 0.004$, paired t-test) (Fig. 3E, Fig S4A). These findings are consistent with the findings of previous studies that reported movement related increases in AP firing in visual thalamic nuclei (Erisken et al., 2014; Petty et al., 2020, Aydın et al., 2018).

At the membrane potential level, whisk onsets were associated with rapid depolarizations in visual thalamic neurons that were reminiscent of the membrane potential depolarizations described above for L2,3 neurons (Fig. 3F). Sorting the membrane potential according to walk onset, in turn, did not reveal such rapid depolarizations in visual thalamic neurons (Fig. 3G). The depolarizations associated with whisk onsets had a median peak response of 4.59 mV [5.53–2.89 IQR], a median 20%−80% rise time of 273.04 ms [394.98–140.35 IQR] and a median half maximum time of 11.05 ms [60.42-(−102.6) IQR], (Fig. 3H–K). In contrast to visual cortical neurons, whisker movement and locomotion did not significantly alter the variability of the membrane potential in visual thalamic neurons (median quiet 7.21 $mV^2$ [9.35–6.68 IQR]; median whisk 8.03 $mV^2$ [9.91–6.23 IQR]; $p = 0.702$, paired t-test) (Fig. 3L,M). This lack of effect on membrane potential variability may result, at least in part, from the finding that the membrane potential of visual thalamic neurons often exhibited depolarization in the absence of whisker pad movements (e.g. Fig. 3D).

These results reveal that the kinetics and the timing of the depolarizations are similarly tightly coupled to whisk onsets in visual thalamic neurons and V1 L2,3 cells. These similarities, in turn, support the possibility that the rapid movement/arousal associated depolarizations in V1 may be regulated/impacted by visual thalamic activity. Future studies, in which the visual receptive field is aligned between visual thalamic neurons and V1 cells during simultaneous recordings will be required to further investigate details regarding the relative timing of movement signals between these structures.

## Alpha-like 3–5 Hz rhythm exhibits rhythmic synaptic and intrinsic membrane potential events

Apart from the rapid whisker pad movement associated depolarizations, another common state-dependent pattern of activity in V1 and visual thalamic neurons was the 3–5 Hz alpha-like oscillation (Fig. 1G, 2C, S1D). Our intracellular recordings in layer 2,3 neurons of V1 (and L4,5,6; Fig. S1D) revealed the 3–5 Hz alpha rhythm to express as an initial hyperpolarization followed by several cycles of depolarization and hyperpolarization (Fig 4A). Closer inspection of these depolarizing events indicated that they consisted of barrages of synaptic potentials, whereas the hyperpolarizing components appeared as a relative reduction in membrane potential variance, suggesting they represent periods of reduced synaptic activity (Fig. 1G, 2C, 4A, S1D). The onset of the 3–5 Hz oscillations was associated on average with reductions in wheel/whisker pad movements and pupil constriction (Fig. 4A). Except for a few outliers, whisker pad movements (including short twitches) occurred before the onset of nearly all of the 3–5 Hz oscillations, and the pupil constricted in about 80% of the cases (Fig. 4B). The median duration of the 3–5 Hz oscillation was about 1 s (Fig. 4C) and the onset of whisker pad movements and of walking were associated with a decreased probability of this oscillation to occur (Fig. 4D,G). This decrease in probability was also reflected in a reduction of FFT power within the 3–5 Hz frequency band indicating that movements onsets diminish the oscillation (Fig. 4D,G). In accordance with the average reduction of movement at the onset of the oscillation (Fig. 4A), we detected a higher probability of the oscillation to occur around whisking- (Fig. 4 E,F) and locomotion- offsets (Fig. 4 H,I) (median probability whisk onset 7.362% [14.643–0 IQR]; median probability whisk offset 28.571% [44.722–14.286 IQR], $p < 0.001$; median

probability walk onset 0% [0.357–0 IQR]; median probability walk offset 6.25% [20.357–0 IQR], $p < 0.001$).

Interestingly, the onset of 3–5 Hz oscillations typically occurred after walking offset, while their distribution around whisking offset was broader (Fig. 4E vs. H). The late occurrence of 3–5 Hz oscillations with walking offset may be due to the presence of strong whisking throughout locomotion, with whisking only decreasing after the cessation of walking (Fig 4H). Together, these results indicate that the oscillation occurs predominantly when motor movements and arousal levels decrease.

Where might the barrages of synaptic activity in cortical neurons originate during the 3–5 Hz rhythm? We hypothesized that these synaptic barrages may originate, at least in part, in the thalamus. Indeed, simultaneous Neuropixels probe recording of multiple neuron activity in either the dLGN or LP with simultaneous whole cell recordings in L2,3 V1 neurons revealed prominent synchronized AP activity in the thalamus that coincided with the barrages of synaptic potentials arriving in visual cortical neurons (Fig. 5A). Furthermore, the initiation of the oscillation was associated with a sudden decrease in thalamic action potential discharge, and a hyperpolarization of cortical neuronal membrane potential (Fig. 5B; n=7 simultaneous recordings). Since we did not align the visual field locations of the simultaneous thalamic/cortical recordings, we did not attempt to compare precise onset times of the 3–5 Hz rhythms between these structures.

Examining the spectral coherence between averaged/summed visual thalamic activity and membrane potential oscillations in V1 revealed a prominent peak at approximately 3–5 Hz (Fig. 5C) indicating a strong relationship between activity in these thalamic nuclei and V1 neuronal membrane potential within this frequency range. By screening our recordings for periods of >100 ms of silence, followed by 2–5 APs with intraburst frequencies of ≥ 250 Hz (a common marker for the occurrence of LTS-mediated burst firing) (Lu et al., 1992), we further found that the 3–5 Hz rhythm was associated with frequent AP burst firing in dLGN and LP units (Fig. 5B), indicating that they are initiated by intrinsic low threshold $Ca^{2+}$ spikes (McCormick and Bal, 1997). We detected at least 1 bout of such AP bursts at an inter-burst frequency of 3–5 Hz during recording sessions in 176 out of 257 dLGN units (~69%), and in 91 out of 146 LP units (~62%) at median rates of 0.01 Hz [0.023–0.004 IQR] and 0.015 Hz [0.028–0.004 IQR] (Fig. 5D). Sorting the membrane potential of V1 neurons to the onset of these bursts revealed that the oscillation coincided in the visual thalamus with rhythmic depolarizations in L2,3 V1 neurons (Fig. 5B,E,F).

Averaged whisker movement activity and wheel movements exhibited a decrease preceding the onset of the 3–5 Hz oscillations in visual thalamic neurons in accordance to our findings described above for the whole-cell recordings (Fig. 5F and Fig. 4A), These findings lend further support to the hypothesis that that this rhythm preferentially occurs during the decrease, or cessation, of enhanced movement – a time when the pupil typically constricts (see also Einstein et al., 2017; Crombie et al., 2021).

We detected the 3–5 Hz oscillations in all 8 intracellularly recorded visual thalamic neurons. At the onset of these oscillations, the membrane potential of dLGN/LP neurons

showed a sudden and pronounced hyperpolarization (median −79.11 mV [−82.07 – (−76.01) IQR] (Fig. 6A–D), which was associated with a decrease in membrane potential variance (Fig. 6C,D). Since decreases in synaptic activity result in a decrease in membrane potential variance, this result suggests that the hyperpolarization is mediated by the sudden withdrawal of depolarizing synaptic barrages. Following this onset-hyperpolarization, the membrane potential slowly, and then suddenly, depolarized (Fig. 6B, Fig. S4D). By using the same criterion as above for identifying putative LTS mediated AP bursts, we found that in 55.6% of the cases during the first oscillation cycle, these depolarizations were associated with burst firing. Preceding these bursts, the membrane potential was significantly more hyperpolarized compared to instances when no bursts were initiated during the first cycle (Fig. 6 E). Furthermore, the APs during the first cycle had a median interspike interval of 3.5 ms [4.32–3.015 IQR] (Fig. S4B) that is consistent with the LTS criterion of ≥250 Hz intraburst frequency and their number correlated with the degree of membrane potential hyperpolarization that preceded the first oscillation cycle (Fig. 6F). Together, these findings strongly support the hypothesis that the AP bursts during the 3–5 Hz alpha-like rhythm are generated via the low-threshold $Ca^{2+}$ spike mechanism (McCormick and Bal., 1997). The sudden depolarization was associated by an increase in membrane potential variance, indicating that it was likely mediated by the arrival of PSP barrages (Fig. 6B–D). The 3–5 Hz oscillation in visual thalamic neurons appeared as several (2–7) cycles of hyperpolarization-depolarization. Often, the depolarizations failed to initiate either a low threshold $Ca^{2+}$ spike or APs. In these cases, the barrage of PSPs arriving in thalamic neurons during this oscillation were clearly observable (Fig. 6B and S4D). Interestingly, in recordings from LP neurons, we observed that these PSPs often contained EPSP-like events that were of larger amplitude (2–10 mV), suggesting they may arise from activity in layer 5 corticothalamic neurons (Sherman, 2016). Gradually, over the course of the oscillation, the hyperpolarized membrane potential lessened, and the oscillation stopped (Fig. 6B,D). Between bouts of 3–5 Hz oscillation, the membrane potential of thalamic neurons frequently exhibited a relatively sustained depolarization, often in the absence of overt movement (Fig. 3D, 6A; Fig. S4C).

## Optogenetic silencing of visual cortex or pharmacological block of visual thalamic activity abolishes the 3–5 Hz rhythm

Based upon our recordings, we hypothesized that the arousal/movement-related changes in thalamic and cortical activity, along with the 3–5 Hz rhythms, may represent thalamocortical interactions. To test this hypothesis, we employed an optogenetic approach whereby activity within visual cortex (VC) was suppressed by stimulating channelrhodopsin expressing PV positive interneurons (Hippenmeyer et al., 2005; Madisen et al., 2012; Speed et al., 2019). In a separate set of experiments, we inactivated the visual thalamus through the injection of fluorescently-coupled muscimol (a potent $GABA_A$ receptor agonist), with the center of the injection site in either dLGN or LP, but typically near the border of these two visual thalamic nuclei (Fig. S7).

Optogenetic activation of PV interneurons in VC suppressed AP activity in putative PV-negative neurons throughout all cortical depths under the center of light delivery (Fig. S5). Although the stimulation was focused on V1 through a relatively small craniotomy (~300

um), we cannot rule out the possibility that other higher visual cortical regions were also affected. For this reason, we refer to this manipulation as silencing of the VC (rather than V1). During the optogenetic silencing of the visual cortex, 3–5 Hz oscillations in the dLGN and LP were abolished (Fig. 6G–I, S4E). Similarly, inactivation of the visual thalamus via the injection of muscimol prevented the occurrence of the 3–5 Hz oscillation in the membrane potential of L2/3 V1 neurons (Fig. 6J,K). Together, these results indicate that the 3–5 Hz oscillation represents a thalamocortical rhythm that depends upon intact interactions between the thalamus and cortex.

### Optogenetic silencing of visual cortex and pharmacological block of visual thalamic activity differentially impact movement related signals in V1 and visual thalamic neurons.

Next, we assessed the consequences visual cortical silencing on movement related signals in visual thalamic neurons, and of visual thalamic inactivation on movement related signals in V1 (Fig. 7, Fig. S6). Upon suppression of activity in visual cortex, we observed that the median activity in dLGN units was suppressed by −46.55% [−1.22-(−6.94) IQR], while LP units showed an even larger median reduction in their activity by −83.26% [−5.33-(−9.68) IQR] (Fig. 7A–C, Fig. S6A–C). These results are consistent with the strong dependence of dLGN neurons upon retinal input, while LP cells appear to be mainly driven by visual cortical activity (Sherman, 2016). In contrast to our results for the 3–5 Hz oscillations, the optogenetic silencing of the visual cortex did not have a uniform effect on whisker movement associated signals in dLGN and LP units (Fig. 7D–I, Fig. S6D–I). About 25% of the units in the dLGN and ~10% of the units in the LP showed a significant increase in whisker movement related signals during visual cortical silencing (Fig. 7F,G Fig. S6F,G). In ~12% of the dLGN units and in ~28% of LP units, whisker movement associated signals were significantly reduced (Fig. 7F,H Fig. S6F,H), which suggests that visual cortical silencing has overall a more negative effect on whisker movement related signals in the LP than in the dLGN. Interestingly, whisker movement associated signals were not significantly changed in 62% of both dLGN and LP neurons (Fig. 7F,I, Fig. S6F,I) indicating that these cells may be modulated by whisker movement independently of the visual cortex. Taken together, these results support the hypothesis that movement-related signals in most visual thalamic cells are not dependent on visual cortical activity and may therefore receive these signals from another brain structure. The 3–5 Hz rhythm on the other hand requires an intact visual cortex, which lends support to the hypothesis that this rhythm may reflect a genuine thalamocortical rhythm.

To further test the role of thalamic activity in regulating whisker movement associated membrane potential depolarizations in visual cortex, we studied state-dependent activity in L2,3 V1 neurons with whole cell recordings while the visual thalamus was silenced via muscimol (Fig. 8, Fig. S7). Previous studies using extracellular recordings showed that silencing of the dLGN reduces higher frequency activity in the visual cortex of awake rodents (Murata and Colonnese 2018; Reinhold et al., 2015), and some evidence suggests that it reduces AP firing associated with movements (Murata and Colonnese 2018). Our results revealed that inactivation of visual thalamic nuclei strongly reduced whisking and locomotion related membrane potential depolarizations in V1 (Fig. 8A,B). Specifically, the median amplitude of the rapid PSP responses at whisk onset was significantly reduced to

5.8 mV [7.3–4.7 IQR, unpaired t-test, p = 0.049] which corresponds to a decrease of ~30% when compared to the control cells shown in Fig. 2 (Fig. 8C). The kinetics of the rapid whisker associated depolarizations remained similar compared to controls with a median half-maximum time of 45.1 ms [58.4–13.1 IQR] (Wilcoxon rank sum test, p = 0.146) and a 20%−80% rise time of 229.2 ms [396.9–109.0 IQR] (Wilcoxon rank sum test; p = 0.234) (Fig. 8E,F). Most strikingly, we observed that the steady-state component of whisker-related signals was almost entirely abolished (median 0.34 mV [0.58-(−0.02) IQR]) when compared to control neurons (median 3.84 mV [5.92–2. IQR] (Wilcoxon rank sum test, p < 0.001) (Fig. 8D). This marked reduction in sustained depolarization with movement following inactivation of the visual thalamus suggests that state-dependent changes of activity in the thalamus are critical to sustain depolarizations associated with arousal/movement related signals in V1.

## Discussion

In the present study, we investigated the role of visual thalamic activity in regulating waking state-dependent activity in V1, with a particular focus on movement/arousal related signals and a 3–5 Hz alpha-like oscillation. Overall, we found that thalamocortical activity plays an essential role in the generation of the 3–5 Hz oscillations and that thalamic activity is necessary to sustain movement/arousal related signals in V1. Finally, we demonstrate that these signals contain a rapid component that is likely mediated via an ionotropic receptor activating pathway that may act, at least in part, independently of movement, per se.

### 3–5 Hz alpha-like oscillations reflect a thalamocortical rhythm that involves LTS mediated AP firing in visual thalamic neurons

By performing whole-cell recordings in L2,3 V1 pyramidal neurons of awake mice, we observed the frequent occurrence of a 3–5 Hz oscillation in the membrane potential (Einstein et al., 2017) (Figs. 1–6). This particular rhythm was previously proposed to constitute an evolutionary precursor of the primate alpha oscillation, and to be associated with pupil constriction, immobility, the offset of visual stimulation and to exhibit the greatest power in LFP in cortical layer 4 (Einstein et al., 2017; Senzai et al., 2019). Our results here demonstrate that this oscillation represents a cyclical thalamocortical interaction, typically associated with decreased movement/arousal, and associated with LTS mediated bursting firing in thalamocortical cells (Fig. 6A–F, Fig. S4). We propose the 3–5 Hz oscillation primarily represents a cyclical thalamocortical interaction based upon: 1) the prevalence of barrages of postsynaptic potentials (PSPs) in both thalamic and cortical neurons with each cycle of the oscillation; 2) the synchronization of these cortical PSPs barrages with AP activity in the thalamus; 3) the initiation of LTSs in thalamic cells by these synaptic barrages (Fig. 6B,C and S4D); and 4) the abolition of this oscillation when activity in either visual cortex or thalamus is blocked (Fig. 6G–K).

We propose that the 3–5 Hz oscillation is generated through the following events: the withdrawal of a sustained depolarizing synaptic activity - such as after movement, or visual stimulation (or, in primates, upon eye closure), or with low levels of vigilance - leads to a pronounced hyperpolarization of visual thalamic and cortical neurons. The

withdrawal of excitatory drive may occur through the failure of corticocortical recurrent drive, such as occurs at the end of an Up state (Compte et al., 2003), through the failure of thalamo-cortico-thalamic interactions to maintain sustained activity, or through the sudden withdrawal of an ionotropic-receptor mediated activating system, such as cholinergic activation mediated through nicotinic receptors (Zagha and McCormick, 2014). The pronounced hyperpolarization removes inactivation of the LTS mechanism in visual thalamic neurons, resulting in a rebound low threshold $Ca^{2+}$ spike mediated burst of action potentials in a subset of these neurons. This low threshold $Ca^{2+}$ spike may be initiated by either depolarization through the activation of the hyperpolarization-activated current (h-current) (McCormick and Bal, 1997) or the arrival of a barrage of synaptic potentials from activity in corticothalamic cells, although both are likely to contribute. This synchronized burst of thalamocortical neuronal activity then drives the visual cortex, resulting in a synchronized discharge of visual cortical neurons, including thalamic projecting layer 5/6 neurons, which reinforce the activity within the visual thalamus. Inactivation of the low threshold $Ca^{2+}$ current in thalamic neurons may then terminate that cycle of the oscillation, resulting, once again, in the hyperpolarization of cortical and thalamocortical neurons, setting the state for the next cycle. The oscillation continues, with each cycle weakening in relation to a decreased intercycle hyperpolarization in thalamocortical neurons, perhaps owing to accumulation of h-current activation (Lüthi and McCormick, 1998), synaptic depression (Chung et al., 2002; Nestvogel et al., 2020), or desynchronization of thalamocortical activity (Wright et al. 2021). The fact that the oscillations typically occur following withdrawal of depolarization associated with the cessation of movement (Figs. 1, 3, 5, 6) is consistent with the properties of the h-current, which is de-activated by depolarization, thereby allowing a strong initial hyperpolarization of thalamocortical neurons with the sudden withdrawal of excitation. Indeed, oscillations based upon interactions of the h-current and the low threshold $Ca^{2+}$ spike mechanism in thalamocortical cells often appear as a damped oscillation remarkably similar to those observed here (see Figs. 9–12 in McCormick and Huguenard, 1992).

The thalamic reticular nucleus (TRN) plays a prominent role in spindle waves during sleep and high-threshold spindles in waking rats (Buzsaki et al., 1988; Fernandez and Lüthi, 2020; McCormick and Bal, 1997; Steriade et al., 1993). The role of the thalamic reticular nucleus in the 3–5 Hz oscillation studied here is as of yet unknown. The possibility that the hyperpolarizing periods in thalamocortical neurons are initiated in part by activation of TRN neurons can be examined in future studies by simultaneous recording of TRN and thalamocortical neurons and determining the reversal potential of the hyperpolarizing and depolarizing cycles of the oscillation in thalamocortical neurons.

How does this hypothesis compare to the results of previous studies? With the increase in brain size, it was previously proposed that the frequency of the alpha rhythm may have increased from 3–5 Hz in the mouse, to 6–12 Hz in cats and to 8–12 Hz in humans (Senzai et al., 2019). Interestingly, some evidence indicates that the alpha oscillation in adult humans develops from a ~4 Hz rhythm in infants, which is within the frequency range of the 3–5 Hz oscillation in mice (Niedermeyer, 1997). It is not clear whether the neural mechanisms that generate the alpha oscillation were conserved in evolution. In cats, it has been proposed that high-threshold mediated AP bursts are associated with alpha rhythms (Crunelli et al., 2018;

Lorincz et al., 2009), which is different to our results of LTS mediated AP bursting during the 3–5 Hz alpha-like rhythm in the mouse (but see Molnár et al., 2021). Interestingly, mice and primates are closer relatives in evolutionary terms than cats and primates, and it remains to be addressed, whether LTS, or high threshold mediated AP bursts are associated with the primate alpha oscillation and whether the degree by which animals are related to each other in evolutionary terms, or the size of the brain is the decisive factor that determines the mechanism of alpha rhythm generation. Although the cell intrinsic mechanisms that are associated with the alpha rhythm may differ in the animal kingdom, it is intriguing to speculate that the overall importance of visual thalamic activity in regulating the alpha rhythm in visual cortical regions may have been conserved across mice, cats and primates (Hughes and Crunelli, 2005; Saalmann et al., 2012). Interestingly, recent studies in mice suggest that the presence of the 3–5 Hz rhythm is disruptive to performing a learned Go/No-Go response to a visual stimulus (Speed et al., 2019), suggesting that it may occur mainly during periods of inattentiveness or may, itself, actively disrupt thalamocortical sensory processing.

### Sustained depolarizations in V1 neurons during movement/arousal correlate with, and require, visual thalamic activity

The second state-dependent activity pattern that we focused on in our study was the rapid change from slowly fluctuating synaptic activity to a steady depolarization in V1 neurons that has been observed in conjunction with locomotion and increases in arousal (Bennett et al., 2013; Polack et al., 2013; Reimer et al., 2014) (Fig. 1). This distinct brain state has also been reported in the primary auditory cortex (A1) (McGinley et al., 2015a; Schneider et al., 2014) and somatosensory cortex (S1) (Poulet and Petersen, 2008; Zagha et al., 2013). Various neural mechanisms have been proposed to regulate this state-dependent activity change including neuromodulation via noradrenergic and cholinergic pathways (Eggermann et al., 2014; Fu et al., 2014; Lee et al., 2014; Polack et al., 2013), changes in the activity of intracortical inhibitory networks (Fu et al., 2014; Pinto et al., 2013; Polack et al., 2013; Reimer et al., 2014), and feedback from secondary and primary motor cortex (Leinweber et al., 2017; Zagha et al., 2013). In addition, studies have shown that inactivation of the somatosensory thalamus abolishes the movement-related steady depolarization in S1 neurons (Poulet et al., 2012), suggesting that thalamic activity may provide the synaptic input necessary for the sustained depolarization in the cortex.

Here we performed a detailed kinetic analysis in L2,3 V1 neurons of the sustained depolarization associated with movement/arousal. Our results revealed a tight coupling of whisker movements with the occurrence of these depolarizations on the scale of tens of milliseconds or less (Fig. 1, Fig. S2M,N), lending support to the hypothesis that these responses are driven in V1 by fast ionotropic signaling. Importantly, similar depolarizations also occurred during pupil dilations in the absence of overt movements of the whisker pad and the running wheel (Fig. S1), suggesting that a significant component of these signals may be associated with changes in arousal rather than movement per se (McGinley et al., 2015a; Petty et al., 2020), with the neural mechanisms of movement adding additional activating and information-containing (e.g. eye position, head direction) signals (Bouvier et al., 2020; Miura and Scanziani, 2021).

Simultaneous extracellular recordings in visual thalamic neurons with whole-cell recordings in V1 additionally revealed that the rapid depolarizations in V1 strongly correlated with visual thalamic activity (Fig. 3). Interestingly, we also found that the membrane potential of visual thalamic neurons exhibited depolarizations with similar kinetics as those of V1 neurons during whisk onsets indicating these two brain structures exhibit remarkable similarities in movement/arousal related state changes on the level of AP firing and postsynaptic activity (Figs. 1H, 2F, 3F). The membrane potential of thalamic neurons is highly regulated by a variety of modulatory neurotransmitters (McCormick, 1992). Currently, the main modulatory systems that can quickly depolarize thalamic neurons is cholinergic activation of nicotinic receptors and corticothalamic activation of glutamatergic ionotropic receptors (McCormick, 1992), although the possible involvement of an additional ionotropic excitatory releasing neurotransmitter system in the observed movement-related thalamic activations cannot be excluded. Relevant to this, recent work suggests that neither reafferent signals from the periphery, the superior colliculus, or cerebral cortex are responsible for state-dependent changes in sensory thalamic activity (Petty et al., 2020; Spacek et al., 2020), although state changes in retinal activity (Liang et al., 2020; Schröder et al., 2020) may contribute to state-dependent activity in the visual thalamus. In addition, fast glutamatergic input from the brainstem may be involved in regulating visual thalamic activity during movements. In support of this, a previous study reported the increased occurrence of fast and large excitatory PSPs in somatosensory thalamic neurons during whisker movements, which are thought to originate from driver inputs from brainstem fibers (Urbain et al., 2015). Furthermore, increased AP firing has been reported in the somatosensory brainstem during whisking (Moore et al., 2015). In contrast to the lack of consistent effect of visual cortical silencing on arousal/movement related changes in the visual thalamus (Fig. 7, Fig S6), silencing of the visual thalamus dramatically affected visual cortical activity by largely abolishing the movement-related steady depolarization (Fig. 8, Fig. S7). Following inhibition of thalamic activity, the only movement-related component remaining in the visual cortex was a transient depolarization at movement onset, which was also reduced in amplitude, but not kinetics (Fig. 8). These results indicate that thalamic activity plays a critical role in sustaining movement/arousal related signals in V1and that there may be additional ionotropic pathways mediating the rapid, transient component.

These results are very similar to the findings of Poulet et al performed using the rodent somatosensory system (Poulet et al., 2012), except for the presence of the residual rapid depolarization at the onset of whisking in our study. We speculate that the transient onset may originate from cortical input by structures such as the primary and secondary motor cortices (Leinweber et al., 2017; Schneider et al., 2014; Zagha et al., 2013), or alternatively from fast nicotinic signaling via cholinergic input from the basal forebrain (Eggermann et al., 2014; Reimer et al., 2016), which in turn may involve the action of brain stem nuclei such as the mesencephalic locomotor region (Lee et al., 2014). Given that our pharmacological injections only partially inactivated the visual thalamus, as indicated by the histological assessment of fluorescent dye at the injection sites (Fig. S7), we cannot rule out the possibility that the residual signal at the onset of the depolarization in V1 during our experiments could also originate from the activity of visual thalamic neurons that were not silenced. Future studies are required to test these possibilities in greater detail, which in

turn may help to better understand the specific contribution of the other previously proposed neural mechanisms to regulating and shaping the movement/arousal related state-changes in V1 and other primary sensory cortices described above (Eggermann et al., 2014; Fu et al., 2014; Leinweber et al., 2017; Polack et al., 2013; Zagha et al., 2013). Based on previous results of the necessity of activity of the somatosensory thalamus for whisker movement related signals in S1 and our similar results in the visual system, we speculate that thalamocortical interactions play an essential mechanistic role in regulating movement/arousal related cortical state changes that is conserved across primary sensory regions.

In rare cases, we observed pupil dilations without motor movements (Fig. S1C) that were associated with membrane potential depolarizations similar to those observed during whisker movements. This finding indicates that movement per se is not required for this phenomenon to occur. Owing to the rare occurrence of pupil dilation events in the absence of movement, we were not able to address the question of whether membrane potential depolarizations also occur at these events in visual thalamic neurons, or in V1 neurons while the visual thalamus is silenced. Future studies will be required to test whether the mechanisms for membrane depolarizations in V1 neurons during pupil dilation in absence of overt movements may be different from those during movements.

Prior studies have demonstrated that visual cortical sensory responses in layer 2/3 neurons are enhanced by locomotion and arousal (Niell and Stryker, 2010; Erisken et al., 2014). Similarly, locomotion has been shown to increase the amplitude of visually evoked responses in dLGN neurons (Erisken et al., 2014; Aidyn et al., 2018). Our findings suggest that this enhancement may result, at least in part, from depolarization of both cortical (Reimer et al., 2014; Polack et al., 2013; Bennett et al., 2013; Neske et al., 2019) and thalamic neurons (present study). The loss of sustained depolarization of visual cortical neurons with movement following inactivation of visual thalamus suggests that this sustained depolarization may arise from movement/arousal-related activation of the thalamus, as has been observed in the somatosensory system (Poulet et al., 2012; Eggermann et al., 2014). Locomotion and arousal have also been shown to impact behavioral performance during visually guided go/no-go tasks, with some results indicating improvements with locomotion (Bennett at al., 2013) and others reporting decreases in performance at high arousal and locomotion (Neske et al., 2019). Clearly, more studies are needed to investigate the effect of movements and arousal on visual system processing.

In summary, our study supports the hypothesis of a crucial role of visual thalamocortical interactions in regulating and shaping recurrent waking state-dependent activity. These state-dependent changes, in turn, have been reported to significantly contribute to the astonishing trial-to-trial variability of sensory and behavioral responses (McCormick et al., 2020; McGinley et al., 2015a, 2015b; Neske et al., 2019; Niell and Stryker, 2010; Speed et al., 2019).

# STAR Methods

## RESOURCE AVAILABILITY

**Lead Contact—**Further information and requests for resources should be directed to and will be fulfilled by the lead contact, David McCormick (davidmc@uoregon.edu).

**Materials Availability—**This study did not generate new unique reagents or mouse lines.

### Data and Code Availability

- Data reported in this paper will be shared by the lead contact upon request.
- All original code has been deposited at Zenodo and is publicly available. The DOI is listed in the key resources table.
- Any additional information required to reanalyze the data reported in this paper is available from the lead contact upon request.

## EXPERIMENTAL MODEL AND SUBJECT DETAILS

All animal procedures were carried out with permission by and in accordance with the regulations of the University of Oregon Institutional Animal Care and Use Committee. The mice used in the present study were kept on a reversed light cycle with free access to food and water. Male and female mice between ages 2 ½ months – 6 months were used for all experiments. The following mouse strains were used in this study: C57BL/6J (JAX, 000664) and PV-cre (+/−) x Ai32 (+/−) (B6.129P2-Pvalb$^{tm1(cre)Arbr}$/J x B6.Cg-Gt(ROSA)26Sor$^{tm32(CAG-COP4*H134R/EYFP)Hze}$/J).

## METHODS DETAILS

**In-vivo Patch Clamp Recordings—**Blind, in vivo whole-cell recordings were performed in the primary visual cortex of adult mice (> 2 months). For this, a craniotomy (~300 μm diameter) was introduced under isoflurane anesthesia at 3 mm posterior of bregma and 2.5 mm lateral to the midline (Lien and Scanziani, 2013). Mice were allowed to recover from surgery for at least 3 hours, before recording. Patch pipettes (4–7 MΩ) were inserted into the brain with an initial positive pressure of 300–400 mbar (for V1 recordings), or at 800 mbar (for thalamic recordings). The pressure was reduced to 30 mbar, upon reaching a depth of ~100 μm for V1 recordings (~2300 μm for thalamic recordings). To search for neurons, the pipette was lowered at 2 μm steps and increases in the pipette resistance were monitored via the application of a test pulse in voltage clamp mode (Margrie et al., 2002). V1 neurons were measured at a depth of 100–350 μm and thalamic cells at a depth of 2300–2700 μm from the pial surface. Successful encounters with cells were followed by the formation of a giga seal at a holding potential of −70 mV and the cell membrane was ruptured via short negative pressure pulses to perform recordings in the whole-cell/current clamp mode (series resistance < 60 mΩ) (Hamill et al., 1981). The intracellular recording solution contained (in mM) 130 K gluconate, 4 KCl, 2 NaCl, 10 HEPES, 0.2 EGTA, 4 ATP-Mg, 0.3 GTP-Na, and 14 phosphocreatine-2K and 2% biocytin adjusted to a pH of 7.4 and at an osmolarity of ~290 mM. The surface of the brain was kept moist during recordings with Ringer's solution (in mM: 145 NaCl, 5 KCl, 1.8

$CaCl_2$, 1 $MgCl_2$, 5 HEPES adjusted to pH 7.4, ~290 mM osmolarity). All whole-cell recordings were carried out using a multiclamp 700B amplifier (Molecular Devices) and signals were sampled at 50 kHz using a Power 1401 digitizer (Cambridge Electronic Design Limited). Putative excitatory neurons were distinguished from inhibitory neurons by their relatively broad AP half-width and a regular firing pattern upon positive current injections (McCormick et al., 1985). The initial recording period, in which the membrane potential was significantly hyperpolarized was excluded from the analysis (McGinley et al., 2015a) and only neurons with more than 400 s of high quality recording time (stable membrane potential, overshooting APs during recording) were included in the analysis. The resting membrane potential was corrected offline for a liquid junction potential of −14 mV (Cruikshank et al., 2007). APs were detected when dV/dt reached a threshold of 25 V/s. For subsequent analyses of postsynaptic potentials during state changes, all APs were removed from the recordings by using a custom-written Matlab script (time window of −1x AP halfwidth + 3.5x AP halfwidth; the name of the script is “getspikes_and_clip_2021” and it can be found at https://doi.org/10.5281/zenodo.5539784) (Nestvogel et al., 2020). The maximum of PSP responses associated with whisker movement and locomotion was identified within a window of −0.5 to +0.5 s from movement onset. The 20% to 80% rise time was identified within a time window of −0.5 to +0.5 s from the peak PSP response. The average steady-state amplitude of depolarizations associated with whisker movement and locomotion were calculated within a time window of 0.5–2 s after motor movement onset. To detect 3–5 Hz oscillations in our membrane potential recordings, we downsampled the raw data from 50 kHz to 40 Hz and applied a sliding window FFT (4s window; 90% overlap; hamming windowing) in Matlab (spectrogram function). The FFT Signal within the frequency range of 3–5 Hz was averaged and periods where it crossed a threshold of mean + 1x standard deviation were considered as potential candidates for the occurrence of the 3–5 Hz rhythm. These candidates were then further subjected to manual curation to exclude candidates that clearly did not fulfill criteria of the 3–5 Hz rhythm (e.g. membrane potential fluctuations that did not contain the sharp rhythmic synaptic potentials typically associated with the oscillation) (analysis script can be found at https://doi.org/10.5281/zenodo.5539784 under the name “entire_recording_alpha_detect_and_pool_2021_2”). All experiments were performed in absence of visual stimulation, except for the recording shown in Fig. S4C,D.

**Extracellular Recordings—**Extracellular recordings were made with Neuropixels probes (Neuropixels 1.0, a.k.a. phase 3b)(Jun et al., 2017). Electrode shanks were coated in Dil or DiO (Vybrant solution, Thermo Fisher Scientific) before recordings to allow the post hoc identification of the recording track. A small craniotomy (~300 μm) was introduced under isoflurane anesthesia at 2.0–2.1 mm posterior of bregma and 2 mm lateral to the midline (for LP recordings), or at 2.5 mm posterior of bregma and 2.3 mm lateral to midline (for dLGN recordings). Mice were allowed to recover for at least 3 hours before electrophysiological recordings began. The surface of the exposed brain was kept moist during experiments with Ringer’s solution as described above. The electrode shanks were lowered with a Sutter Instruments micromanipulator at low speed (~2–3 μm per seconds) until a depth of 3600–4000 μm was reached. Recordings were performed after a minimum of 15 min of reaching the final depth at a gain of 250 (LFP), and 500 (APs) with the open-ephys software. All extracellular recording data was acquired using a PXIe acquisition module by National

Instruments. A sync signal was sent from the acquisition module to the Power 1401 digitizer in order to synchronize Neuropixels data with patch clamp recordings and camera frames. The Neuropixels data was sampled at a setting of 30 kHz, but we detected slight deviations from this number offline (~ e.g. actual rate for one recording 29999.795 Hz). All recordings were analyzed at the actual sampling rate. Thalamic AP burst firing was detected with interspike intervals of less than 4 ms (>250 Hz) preceded by more than 100 ms of AP quiescence.

**Videography and Movement Analysis—**All recordings were carried out in head-fixed mice that were positioned unto a cylindrical wheel. Movements of the running wheel (Fig.1) were monitored using a rotary encoder (Encoder Products CO.; 15T-01SF-2500NV1RPP-F03-S1). Signals from the rotary encoder were translated online into units of cm/s with LabView software at a rate of 100 Hz and recorded via a Power 1401 digitizer at 25 kHz. A moving average filter of 20 ms was applied to the 25 kHz data offline to smooth the recorded signal (‘smooth’-function in Matlab). To monitor changes in pupil size and whisker pad movements, the body and the eyes of the mouse were illuminated by infrared light, which was present in addition to a constant ambient light in the room. The anterior half of the animal’s body was monitored via videography using a FLIR Grasshopper 3 camera with FlyCapture2 software (FLIR). A Power 1401 digitizer triggered frame acquisition at a rate of 125 Hz. The exposure times of the camera (i.e. shutter open time; set to 3 ms) were recorded at a rate of 25 kHz via the Power 1401 digitizer. The area of the pupil was determined offline with FaceMap (Stringer et al., 2019), or DeepLabCut (Nath et al., 2019). In a next step, values obtained for the pupil area were assigned to the offset times of the camera exposure signals. The motion energy of whisker pad movements was calculated with a custom Matlab script by subtracting the sum of the absolute pixel intensity of each frame from that of the preceding frame (the script can be found at https://doi.org/10.5281/zenodo.5539784 under the name “whisk_motion_energy”. The timepoints of these values were assigned to be halfway between the two corresponding camera exposure offset times during data analysis. The ‘interp1’ function of Matlab was used to perform linear interpolation for pupil area and whisker pad motion energy datapoints. A whisker movement-bout was defined by the absolute motion energy reaching a threshold of 1 (a.u.) and staying above the threshold for at least 2 seconds. Neighboring whisker movement-bouts that occurred within 1 s or less were grouped together. Similarly, locomotion was defined by the wheel velocity reaching a threshold of 1 cm/s and lasting for at least 1 s. Neighboring locomotion-bouts that occurred within 1 s or less were grouped together. We also ran all analyses treating the variables identically (i.e. downsampling the whisker trace to 100 Hz & no smoothing of the wheel signals & no linear interpolation for whisker motion energy [“sample and hold” for both walking and whisking]). These analyses yielded similar significant results as reported in the manuscript when these signals were used for timing alignment.

**Immunohistochemistry and Microscopy—**Following electrophysiological recordings, mice were deeply anesthetized and subjected to whole-animal perfusion using phosphate buffer (PB) and PB supplemented with 4% paraformaldehyde (PFA). Brains were removed afterward and placed in 4% PFA for at least one night. Brain slices (200 μm thickness) were prepared by using a cryostat after brains were washed 3 times with PB and after

being placed consecutively in 20% and 30% sucrose solution. Before immunostainings, brain slices were incubated at room temperature in 3% Triton-X PB solution. The brain slices were then transferred into a 3% Triton-X PB solution supplemented with Alexa Fluor 555 streptavidin (1:1000, Thermo Fisher Scientific) and DAPI (1:1000, Thermo Fisher Scientific) and incubated at room temperature for an additional 4 hours. In the last step, brain slices were washed 2–3 times with PB (20–30 min) and mounted onto glass microscope slides for subsequent imaging. Microscopy was performed using a CSU-W1 SORA spinning disk microscope (Nikon) equipped with a 4x and a 60x (water) objective.

**Pharmacological and Optogenetic Silencing of dLGN and V1—**A volume of 300 nL fluorophore-coupled muscimol (Bodipy, Thermo Fisher Scientific) was injected into the visual thalamus (2400–2600 μm depth; 2.0–2.3 mm lateral to midline and 2.0–2.5 mm posterior to bregma) at a rate of 60 nL/min at a concentration of 2 mM using a Nanoliter 2020 system (WPI). Optogenetic silencing of V1 was achieved by the use of mice in which channelrhodopsin-2 expression was driven by *cre* in parvalbumin positive interneurons (Ai32 x PVcre). A craniotomy with a diameter of ~300 μm was introduced above V1 (2.5 mm lateral to midline and 3 mm posterior to bregma), while mice were under isoflurane anesthesia. During the electrophysiology recordings, an optical monofiber (0.63 NA) was positioned in close proximity to the craniotomy (1 mm above the dura) and light pulses at 9 mW (at fiber tip) and a duration of 8 s were applied (LEDD1B- T-Cube LED driver, Thorlabs; Connectorized LED 465 nm, Doric Lenses) under the control of CED Spike2 software. Single light pulses were separated by 4 s and 30 s to study the impact of silencing V1 activity on state-dependent activity in the LP and dLGN. Although our optogenetic stimulation was centered around V1, we do not rule out the possibility that other areas surrounding V1 may have partially been stimulated, for which reason we refer to this manipulation as a silencing of the visual cortex. We excluded the first 2 s after optogenetic stimulus onset in our data analysis, as well as the first 2 s following the stimulus offset in order to avoid contamination of neural activity associated with stimulus transients.

**Analysis of data obtained with Neuropixels probes—**All extracellular data obtained with Neuropixels were preprocessed using common-average referencing (https://github.com/cortex-lab/spikes/tree/master/preprocessing)(Steinmetz et al., 2019). After preprocessing, spikes were sorted with Kilosort2 (https://github.com/MouseLand/Kilosort) (Pachitariu et al. 2016). Putative single units that were identified by kilosort2 were subjected to manual curating with phy2. During manual curation, each unit was inspected for potential refractory contaminations, robustness of waveform during recording, similarity of waveform to other units and sudden loss of spiking events during recording. Those units, which passed the quality assessment were labeled as single units and were included in the analysis. Only units with an average spike rate of greater than 0.2 spikes/s were included in the analysis. The depth of neuropixel probes was later matched with the microscopic confocal images to identify dLGN and LP units. For this, we first identified the border between the hippocampus CA3 region and the visual thalamus in our electrophysiology recordings, which was characterised by a large gap of no unit activity. By using the scalable brain atlas by the Allen Institute (Allen Mouse brain common coordinate framework version 3) as an aid, we next measured the length of the DiI-stained track spanning the corresponding

visual thalamic region in the microscopy images and related this information to the depth of electrophysiological recordings to identify the border between visual thalamic regions and neighboring deeper regions (e.g. PoM). Due to tissue shrinkage during PFA fixation, we assumed that this approach would exclude some units that laid in deeper regions of visual thalamic regions. The posthoc analysis of fluorescent electrode tracks also allowed us to identify whether the recordings were performed in the dLGN, or the LP. To determine the spectral coherence between the membrane potential of V1 neurons and visual thalamic activity (average activity of all units per recording), we made use of a previously published Matlab script (Kramer, 2013) with an overlap of 90% and a sliding window of 20s. Averaged dLGN and LP single unit activity was obtained by sorting spikes into 25 ms bins (Fig. 2), or 50 ms bins (Fig.7 and Fig.S6) (no filtering or smoothing was applied). For averaged spiking activity during quiet vs. whisking, (or optogenetic stimulation on vs. off) AP spiking rates were calculated for each respective epoch without binning (e.g. whisker bout). To calculate wavelet coherence for the figures shown in 5A and F, we used the *wcoherence* function in Matlab. The visual receptive fields of V1 neurons and visual thalamic units were not measured during the simultaneous Neuropixels and whole-cell recordings.

### QUANTIFICATION AND STATISTICAL ANALYSIS

All data was tested for normality using the Lilliefors test in Matlab 2019b. For normally distributed datasets we employed the paired t-test (ttest in Matlab), or the unpaired t-test (ttest2 in Matlab) where it was appropriate. For non-parametric data sets, we used the Wilcoxon signed rank sum test (signrank in Matlab), or the Wilcoxon rank sum test (ranksum in Matlab). For multiple comparisons, we made use of the Kruskal-Wallis test (kruskalwallis in Matlab) together with Bonferroni correction (multcompare, ‘CType’, ‘bonferroni’ in Matlab). All 95% confidence intervals shown in graphs were obtained by bootstrapping. To obtain 95% bootstrapped confidence intervals, we randomly resampled the raw data with replacement to calculate a bootstrapped group of means (n = 1000). The confidence intervals reflect 95% of this bootstrapped group. Bootstrapping was also performed for Fig 6,7 F to perform statistical testing on datasets. Differences were deemed to be significant, when the 95% bootstrapped confidence intervals did not cross the reference line (m = 1) in the corresponding plots. Boxplots in figures show the median with the interquartile ranges (IQR). The IQRs in text and figures reflect the 25th and 75th percentiles (Matlab function: prctile(x, [25 75],’all’). The values in the text indicate the median and IQRs. Information about the statistical tests used, the number of neurons/units (= n) and number of animals (= N) can be found in the figure legends.

## Supplementary Material

Refer to Web version on PubMed Central for supplementary material.

## Acknowledgements

We thank Cristopher Niell and Daniel Hulsey for helpful comments on the manuscript and Rennie Kendrick and Kevin Zumwalt for technical assistance. We also thank Laura Boddington, Lindsay Collins, Brett Emmanuel, Suh Yun Jo, Paul Steffan and Evan Vickers for helpful discussions. This work was supported by NIH grants R35NS097287 and R01NS118461.

## References


Aydın Ç, Couto J, Giugliano M, Farrow K, and Bonin V (2018). Locomotion modulates specific functional cell types in the mouse visual thalamus. Nat. Commun 9, 4882. [PubMed: 30451819]

Bennett C, Arroyo S, and Hestrin S (2013). Subthreshold mechanisms underlying state-dependent modulation of visual responses. Neuron 80, 350–357. [PubMed: 24139040]

Berger H (1929). Über das Elektrenkephalogramm des Menschen. Archiv f. Psychiatrie 87, 527–570.

Blot A, Roth MM, Gasler I, Javadzadeh M, Imhof F, and Hofer SB (2021). Visual intracortical and transthalamic pathways carry distinct information to cortical areas. Neuron 109, 1996–2008.e6. [PubMed: 33979633]

Bouvier G, Senzai Y, and Scanziani M (2020). Head Movements Control the Activity of Primary Visual Cortex in a Luminance-Dependent Manner. Neuron 108, 500–511.e5. [PubMed: 32783882]

Buzsaki G, Bickford RG, Ponomareff G, Thal LJ, Mandel R, and Gage FH (1988). Nucleus basalis and thalamic control of neocortical activity in the freely moving rat. J. Neurosci 8, 4007–4026. [PubMed: 3183710]

Chung S, Li X, and Nelson SB (2002). Short-term depression at thalamocortical synapses contributes to rapid adaptation of cortical sensory responses in vivo. Neuron 34, 437–446. [PubMed: 11988174]

Compte A, Sanchez-Vives MV, McCormick DA, and Wang X-J (2003). Cellular and network mechanisms of slow oscillatory activity (<1 Hz) and wave propagations in a cortical network model. J. Neurophysiol 89, 2707–2725. [PubMed: 12612051]

Crombie D, Spacek MA, Leibold C, and Busse L Modulation of dLGN firing mode across multiple timescales is predicted by pupil size dynamics (2021). 10.1101/2021.04.30.442134

Cruikshank SJ, Lewis TJ, and Connors BW (2007). Synaptic basis for intense thalamocortical activation of feedforward inhibitory cells in neocortex. Nat. Neurosci 10, 462–468. [PubMed: 17334362]

Crunelli V, Lőrincz ML, Connelly WM, David F, Hughes SW, Lambert RC, Leresche N, and Errington AC (2018). Dual function of thalamic low-vigilance state oscillations: rhythm-regulation and plasticity. Nat. Rev. Neurosci 19, 107–118. [PubMed: 29321683]

Dolensek N, Gehrlach DA, Klein AS, and Gogolla N (2020). Facial expressions of emotion states and their neuronal correlates in mice. Science 368, 89–94. [PubMed: 32241948]

Eggermann E, Kremer Y, Crochet S, and Petersen CCH (2014). Cholinergic signals in mouse barrel cortex during active whisker sensing. Cell Rep. 9, 1654–1660. [PubMed: 25482555]

Einstein M (2017). Behavioral State Modulates Primary Visual Cortex Responsiveness in Mice. University of California, Los Angeles

Einstein MC, Polack P-O, Tran DT, and Golshani P (2017). Visually Evoked 3–5 Hz Membrane Potential Oscillations Reduce the Responsiveness of Visual Cortex Neurons in Awake Behaving Mice. J. Neurosci 37, 5084–5098. [PubMed: 28432140]

Erisken S, Vaiceliunaite A, Jurjut O, Fiorini M, Katzner S, and Busse L (2014). Effects of locomotion extend throughout the mouse early visual system. Curr. Biol 24, 2899–2907. [PubMed: 25484299]

Fernandez LMJ, and Lüthi A (2020). Sleep Spindles: Mechanisms and Functions. Physiol. Rev 100, 805–868. [PubMed: 31804897]

Fu Y, Tucciarone JM, Espinosa JS, Sheng N, Darcy DP, Nicoll RA, Huang ZJ, and Stryker MP (2014). A cortical circuit for gain control by behavioral state. Cell 156, 1139–1152. [PubMed: 24630718]

Halgren M, Ulbert I, Bastuji H, Fabó D, Erőss L, Rey M, Devinsky O, Doyle WK, Mak-McCully R, Halgren E, et al. (2019). The generation and propagation of the human alpha rhythm. Proc. Natl. Acad. Sci. U. S. A 116, 23772–23782. [PubMed: 31685634]

Hamill OP, Marty A, Neher E, Sakmann B, and Sigworth FJ (1981). Improved patch-clamp techniques for high-resolution current recording from cells and cell-free membrane patches. Pflügers Archiv - European Journal of Physiology 391, 85–100. [PubMed: 6270629]

Hippenmeyer S, Vrieseling E, Sigrist M, Portmann T, Laengle C, Ladle DR, and Arber S (2005). A developmental switch in the response of DRG neurons to ETS transcription factor signaling. PLoS Biol 3, e159. [PubMed: 15836427]

Hughes SW, and Crunelli V (2005). Thalamic mechanisms of EEG alpha rhythms and their pathological implications. Neuroscientist 11, 357–372. [PubMed: 16061522]

Hughes SW, Lörincz M, Cope DW, Blethyn KL, Kékesi KA, Parri HR, Juhász G, and Crunelli V (2004). Synchronized oscillations at alpha and theta frequencies in the lateral geniculate nucleus. Neuron 42, 253–268. [PubMed: 15091341]

Ito S, Feldheim DA, and Litke AM (2017). Segregation of Visual Response Properties in the Mouse Superior Colliculus and Their Modulation during Locomotion. J. Neurosci 37, 8428–8443. [PubMed: 28760858]

Jun JJ, Steinmetz NA, Siegle JH, Denman DJ, Bauza M, Barbarits B, Lee AK, Anastassiou CA, Andrei A, Aydın Ç, et al. (2017). Fully integrated silicon probes for high-density recording of neural activity. Nature 551, 232–236. [PubMed: 29120427]

Kramer MA An introduction to field analysis techniques (2013): The power spectrum and coherence. In The Science of Large Data Sets: Spikes Fields, and Voxels J,E, Ed.; Society for Neuroscience: Washington, DC, USA; pp. 18–25.

Lee AM, Hoy JL, Bonci A, Wilbrecht L, Stryker MP, and Niell CM (2014). Identification of a brainstem circuit regulating visual cortical state in parallel with locomotion. Neuron 83, 455–466. [PubMed: 25033185]

Leinweber M, Ward DR, Sobczak JM, Attinger A, and Keller GB (2017). A Sensorimotor Circuit in Mouse Cortex for Visual Flow Predictions. Neuron 96, 1204.

Liang L, Fratzl A, Reggiani JDS, El Mansour O, Chen C, and Andermann ML (2020). Retinal Inputs to the Thalamus Are Selectively Gated by Arousal. Curr. Biol 30, 3923–3934.e9. [PubMed: 32795442]

Lien AD, and Scanziani M (2013). Tuned thalamic excitation is amplified by visual cortical circuits. Nat. Neurosci. 16, 1315–1323. [PubMed: 23933748]

Lorincz ML, Kékesi KA, Juhász G, Crunelli V, and Hughes SW (2009). Temporal framing of thalamic relay-mode firing by phasic inhibition during the alpha rhythm. Neuron 63, 683–696. [PubMed: 19755110]

Lu SM, Guido W, and Sherman SM (1992). Effects of membrane voltage on receptive field properties of lateral geniculate neurons in the cat: contributions of the low-threshold Ca2+ conductance. J. Neurophysiol 68, 2185–2198. [PubMed: 1337104]

Lüthi A, and McCormick DA (1998). H-current: properties of a neuronal and network pachpacemaker. Neuron 21, 9–12. [PubMed: 9697847]

Madisen L, Mao T, Koch H, Zhuo J-M, Berenyi A, Fujisawa S, Hsu Y-WA, Garcia AJ 3rd, Gu X, Zanella S, et al. (2012). A toolbox of Cre-dependent optogenetic transgenic mice for light-induced activation and silencing. Nat. Neurosci 15, 793–802. [PubMed: 22446880]

Mathis A, Mamidanna P, Cury KM, Abe T, Murthy VN, Mathis MW, and Bethge M (2018). DeepLabCut: markerless pose estimation of user-defined body parts with deep learning. Nat. Neurosci 21, 1281–1289. [PubMed: 30127430]

Margrie TW, Brecht M, and Sakmann B (2002). In vivo, low-resistance, whole-cell recordings from neurons in the anaesthetized and awake mammalian brain. Pflugers Arch. 444, 491–498. [PubMed: 12136268]

McCormick DA (1992). Neurotransmitter actions in the thalamus and cerebral cortex and their role in neuromodulation of thalamocortical activity. Prog. Neurobiol 39, 337–388. [PubMed: 1354387]

McCormick DA, and Bal T (1997). Sleep and arousal: thalamocortical mechanisms. Annu. Rev. Neurosci 20, 185–215. [PubMed: 9056712]

McCormick DA, Connors BW, Lighthall JW, and Prince DA (1985). Comparative electrophysiology of pyramidal and sparsely spiny stellate neurons of the neocortex. J. Neurophysiol 54, 782–806. [PubMed: 2999347]

McCormick DA, Nestvogel DB, and He BJ (2020). Neuromodulation of Brain State and Behavior. Annu. Rev. Neurosci 43, 391–415. [PubMed: 32250724]

McCormick DA, and Huguenard JR (1992). A model of the electrophysiological properties of thalamocortical relay neurons. J. Neurophysiol 68, 1384–1400. [PubMed: 1331356]

McGinley MJ, David SV, and McCormick DA (2015a). Cortical Membrane Potential Signature of Optimal States for Sensory Signal Detection. Neuron 87, 179–192. [PubMed: 26074005]

McGinley MJ, Vinck M, Reimer J, Batista-Brito R, Zagha E, Cadwell CR, Tolias AS, Cardin JA, and McCormick DA (2015b). Waking State: Rapid Variations Modulate Neural and Behavioral Responses. Neuron 87, 1143–1161. [PubMed: 26402600]

Miura SK, and Scanziani M Erasing motion: Scrambling direction selectivity in visual cortex during saccades. (2021) 10.1101/2021.03.30.437338

Molnár B, Sere P, Bordé S, Koós K, Zsigri N, Horváth P, and Lőrincz ML (2021). Cell Type-Specific Arousal-Dependent Modulation of Thalamic Activity in the Lateral Geniculate Nucleus. Cereb Cortex Commun 2, tgab020 [PubMed: 34296165]

Moore JD, Mercer Lindsay N, Deschênes M, and Kleinfeld D (2015). Vibrissa Self-Motion and Touch Are Reliably Encoded along the Same Somatosensory Pathway from Brainstem through Thalamus. PLoS Biol. 13, e1002253. [PubMed: 26393890]

Murata Y, and Colonnese MT (2018). Thalamus Controls Development and Expression of Arousal States in Visual Cortex. J. Neurosci 38, 8772–8786. [PubMed: 30150360]

Musall S, Kaufman MT, Juavinett AL, Gluf S, and Churchland AK (2019). Single-trial neural dynamics are dominated by richly varied movements. Nat. Neurosci 22, 1677–1686. [PubMed: 31551604]

Nath T, Mathis A, Chen AC, Patel A, Bethge M, and Mathis MW (2019). Using DeepLabCut for 3D markerless pose estimation across species and behaviors. Nat. Protoc 14, 2152–2176. [PubMed: 31227823]

Neske GT, Nestvogel D, Steffan PJ, and McCormick DA (2019). Distinct Waking States for Strong Evoked Responses in Primary Visual Cortex and Optimal Visual Detection Performance. J. Neurosci 39, 10044–10059. [PubMed: 31672787]

Nestvogel DB, Merino RM, Leon-Pinzon C, Schottdorf M, Lee C, Imig C, Brose N, and Rhee J-S (2020). The Synaptic Vesicle Priming Protein CAPS-1 Shapes the Adaptation of Sensory Evoked Responses in Mouse Visual Cortex. Cell Rep. 30, 3261–3269.e4. [PubMed: 32160535]

Niedermeyer E (1997). Alpha rhythms as physiological and abnormal phenomena. Int. J. Psychophysiol 26, 31–49. [PubMed: 9202993]

Niell CM, and Stryker MP (2010). Modulation of visual responses by behavioral state in mouse visual cortex. Neuron 65, 472–479. [PubMed: 20188652]

Pachitariu M, Steinmetz N, Kadir S, Carandini M, and Kilosort D,HK: realtime spike-sorting for extracellular electrophysiology with hundreds of channels (2016). 10.1101/061481

Petty GH, Kinnischtzke AK, Kate Hong Y, and Bruno RM Effects of arousal and movement on secondary somatosensory and visual thalamus (2020). 10.1101/2020.03.04.977348

Pinto L, Goard MJ, Estandian D, Xu M, Kwan AC, Lee S-H, Harrison TC, Feng G, and Dan Y (2013). Fast modulation of visual perception by basal forebrain cholinergic neurons. Nat. Neurosci 16, 1857–1863. [PubMed: 24162654]

Polack P-O, Friedman J, and Golshani P (2013). Cellular mechanisms of brain state-dependent gain modulation in visual cortex. Nat. Neurosci 16, 1331–1339. [PubMed: 23872595]

Poulet JFA, and Petersen CCH (2008). Internal brain state regulates membrane potential synchrony in barrel cortex of behaving mice. Nature 454, 881–885. [PubMed: 18633351]

Poulet JFA, Fernandez LMJ, Crochet S, and Petersen CCH (2012). Thalamic control of cortical states. Nat. Neurosci 15, 370–372. [PubMed: 22267163]

Reimer J, Froudarakis E, Cadwell CR, Yatsenko D, Denfield GH, and Tolias AS (2014). Pupil fluctuations track fast switching of cortical states during quiet wakefulness. Neuron 84, 355–362. [PubMed: 25374359]

Reimer J, McGinley MJ, Liu Y, Rodenkirch C, Wang Q, McCormick DA, and Tolias AS (2016). Pupil fluctuations track rapid changes in adrenergic and cholinergic activity in cortex. Nat. Commun 7, 13289. [PubMed: 27824036]

Reinhold K, Lien AD, and Scanziani M (2015). Distinct recurrent versus afferent dynamics in cortical visual processing. Nat. Neurosci 18, 1789–1797. [PubMed: 26502263]

Rossant C, Kadir SN, Goodman DFM, Schulman J, Hunter MLD, Saleem AB, Grosmark A, Belluscio M, Denfield GH, Ecker AS, et al. (2016). Spike sorting for large, dense electrode arrays. Nat. Neurosci 19, 634–641. [PubMed: 26974951]

Roth MM, Dahmen JC, Muir DR, Imhof F, Martini FJ, and Hofer SB (2016). Thalamic nuclei convey diverse contextual information to layer 1 of visual cortex. Nat. Neurosci 19, 299–307. [PubMed: 26691828]

Saalmann YB, Pinsk MA, Wang L, Li X, and Kastner S (2012). The pulvinar regulates information transmission between cortical areas based on attention demands. Science 337, 753–756. [PubMed: 22879517]

Salkoff DB, Zagha E, McCarthy E, and McCormick DA (2020). Movement and Performance Explain Widespread Cortical Activity in a Visual Detection Task. Cereb. Cortex 30, 421–437. [PubMed: 31711133]

Savier EL, Chen H, and Cang J (2019). Effects of Locomotion on Visual Responses in the Mouse Superior Colliculus. J. Neurosci 39, 9360–9368. [PubMed: 31570535]

Schmid MC, Singer W, and Fries P (2012). Thalamic Coordination of Cortical Communication. Neuron 75, 551–552. [PubMed: 22920248]

Schneider DM, Nelson A, and Mooney R (2014). A synaptic and circuit basis for corollary discharge in the auditory cortex. Nature 513, 189–194. [PubMed: 25162524]

Schröder S, Steinmetz NA, Krumin M, Pachitariu M, Rizzi M, Lagnado L, Harris KD, and Carandini M (2020). Arousal Modulates Retinal Output. Neuron 107, 487–495.e9. [PubMed: 32445624]

Senzai Y, Fernandez-Ruiz A, and Buzsáki G (2019). Layer-Specific Physiological Features and Interlaminar Interactions in the Primary Visual Cortex of the Mouse. Neuron 101, 500–513.e5. [PubMed: 30635232]

Sherman SM (2016). Thalamus plays a central role in ongoing cortical functioning. Nature Neuroscience 19, 533–541. [PubMed: 27021938]

Silva LR, Amitai Y, and Connors BW (1991). Intrinsic oscillations of neocortex generated by layer 5 pyramidal neurons. Science 251, 432–435. [PubMed: 1824881]

Spacek MA, Born G, Crombie D, Bauer Y, Liu X, Katzner S, and Busse L (2020). Robust effects of corticothalamic feedback during naturalistic visual stimulation. BioRxiv 776237

Speed A, Del Rosario J, Burgess CP, and Haider B (2019). Cortical State Fluctuations across Layers of V1 during Visual Spatial Perception. Cell Rep. 26, 2868–2874.e3. [PubMed: 30865879]

Steinmetz NA, Zatka-Haas P, Carandini M, and Harris KD (2019). Distributed coding of choice, action and engagement across the mouse brain. Nature 576, 266–273. [PubMed: 31776518]

Steriade M, McCormick DA, and Sejnowski TJ (1993). Thalamocortical oscillations in the sleeping and aroused brain. Science 262, 679–685. [PubMed: 8235588]

Stringer C, Pachitariu M, Steinmetz N, Reddy CB, Carandini M, and Harris KD (2019). Spontaneous behaviors drive multidimensional, brainwide activity. Science 364, 255. [PubMed: 31000656]

Urbain N, Salin PA, Libourel P-A, Comte J-C, Gentet LJ, and Petersen CCH (2015). Whisking-Related Changes in Neuronal Firing and Membrane Potential Dynamics in the Somatosensory Thalamus of Awake Mice. Cell Rep. 13, 647–656. [PubMed: 26489463]

Wright NC, Borden PY, Liew YJ, Bolus MF, Stoy WM, Forest CR, and Stanley GB (2021). Rapid Cortical Adaptation and the Role of Thalamic Synchrony during Wakefulness. J. Neurosci 41, 5421–5439. [PubMed: 33986072]

Zagha E, and McCormick DA (2014). Neural control of brain state. Curr. Opin. Neurobiol 29, 178–186. [PubMed: 25310628]

Zagha E, Casale AE, Sachdev RNS, McGinley MJ, and McCormick DA (2013). Motor cortex feedback influences sensory processing by modulating network state. Neuron 79, 567–578. [PubMed: 23850595]

## Highlights

- Whisker movements correlate with rapid synaptic activity in V1 and visual thalamus
- Silencing of V1 does not abolish movement related activity in most dLGN or LP cells
- Silencing of visual thalamus strongly reduces movement related activation in V1
- Thalamocortical interactions generate state-dependent alpha frequency oscillation

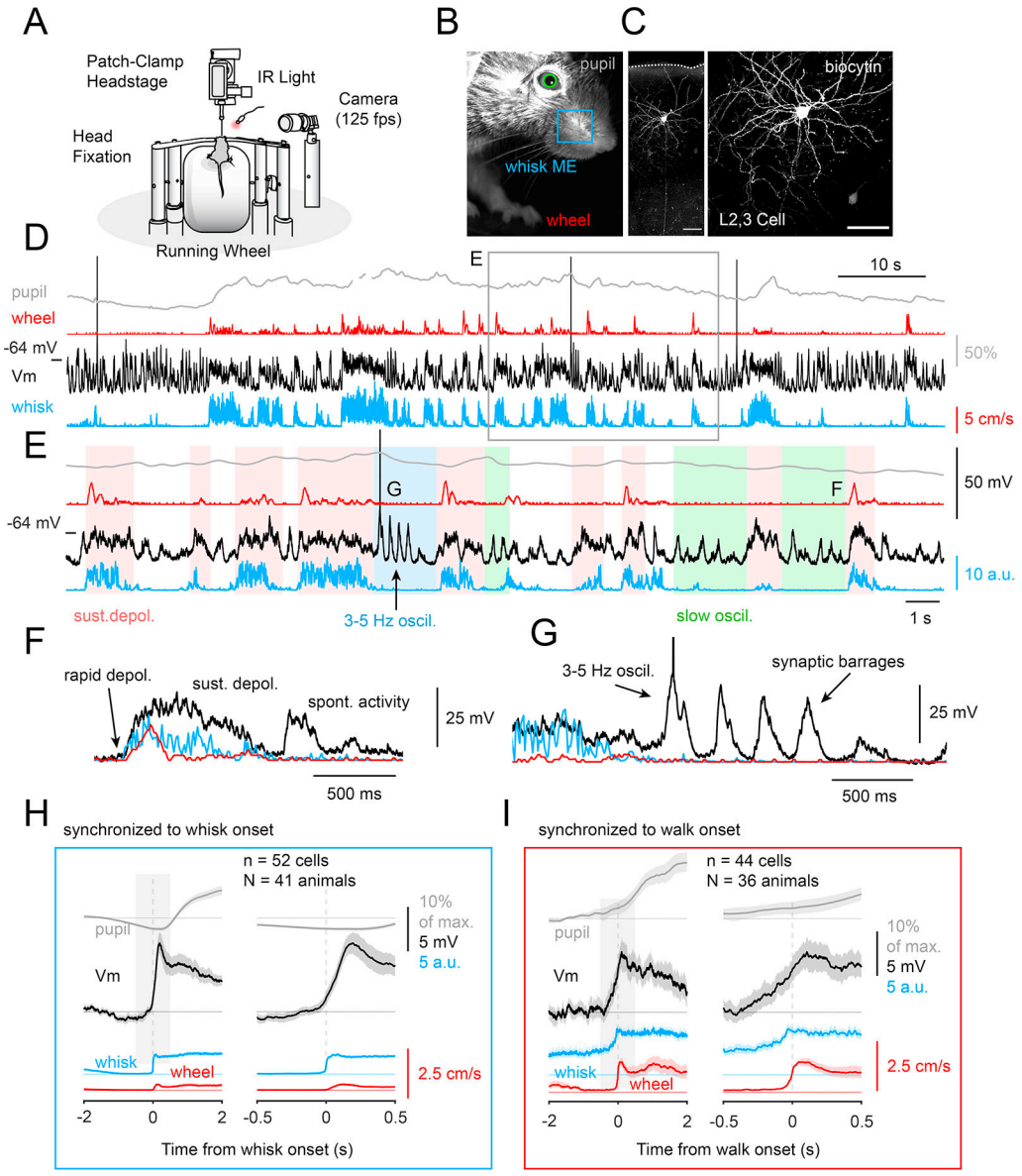


**Figure 1. Whole cell recordings from excitatory L2,3 V1 neurons reveal multiple states of synaptic activity.**

(A) Depiction of experimental setup. The mouse is head-fixed on top of a running cylinder and imaged with infrared light and a camera operating at 125 frames per second. (B) Image of the mouse's face from the video stream (whisk ME = whisker pad motion energy). The blue box indicates the region used to measure whisk ME. (C) Layer 2/3 pyramidal cell recorded and labeled with biocytin. Scale bars indicate 50 μm. (D) Example whole cell recording from the cell in C. Pupil, whisker pad and wheel movement are also illustrated. Note that sometimes the mouse whisks without walking, but always whisks while walking. Note also in this example recording that 3–5 Hz oscillations often appear at the end of a movement bout. Pupil diameter follows movement on a slow (seconds) time scale. The membrane potential of this cortical cell depolarizes strongly whenever the animal moves its whisker pad. (E) Expanded time base of a portion of the traces in D illustrating the

different phases of activity in this cortical neuron. During the periods labeled in pink, the animal's whiskers are moving, which is associated with a strong depolarization of neuronal membrane potential. During the blue period, the 3–5 Hz oscillation is present, and this often occurs after the cessation of walking. During the unlabeled periods, periodic barrages of synaptic activity recur at lower (<2 Hz) frequencies. (F) Overlay of the onset of an example bout of whisker movement, walking, and membrane potential illustrating the rapid onset kinetics of the depolarization. Whisker movement precedes walking and appears to be nearly simultaneous with cortical depolarization. (G) Expansion of a 3–5 Hz oscillation illustrating the marked barrages of synaptic activity arriving in this neuron, and the relationship with the cessation of whisker movement. (H) Alignment of intracellular recordings of cortical neurons to the onset of whisker movement-bouts reveals a sharp synchronized onset of depolarization (two time scales, left and right; n = 52 neurons; N = 41 mice). (I) Alignment of the intracellular recordings to the onset of locomotion reveals less precise alignment (two time scales illustrated; n = 44 cells in N = 36 mice; only recordings during which the mice exhibited at least 1 locomotion bout were included). Shaded regions in graphs indicate 95% bootstrapped confidence interval. See also Figures S1, S2 and S3.

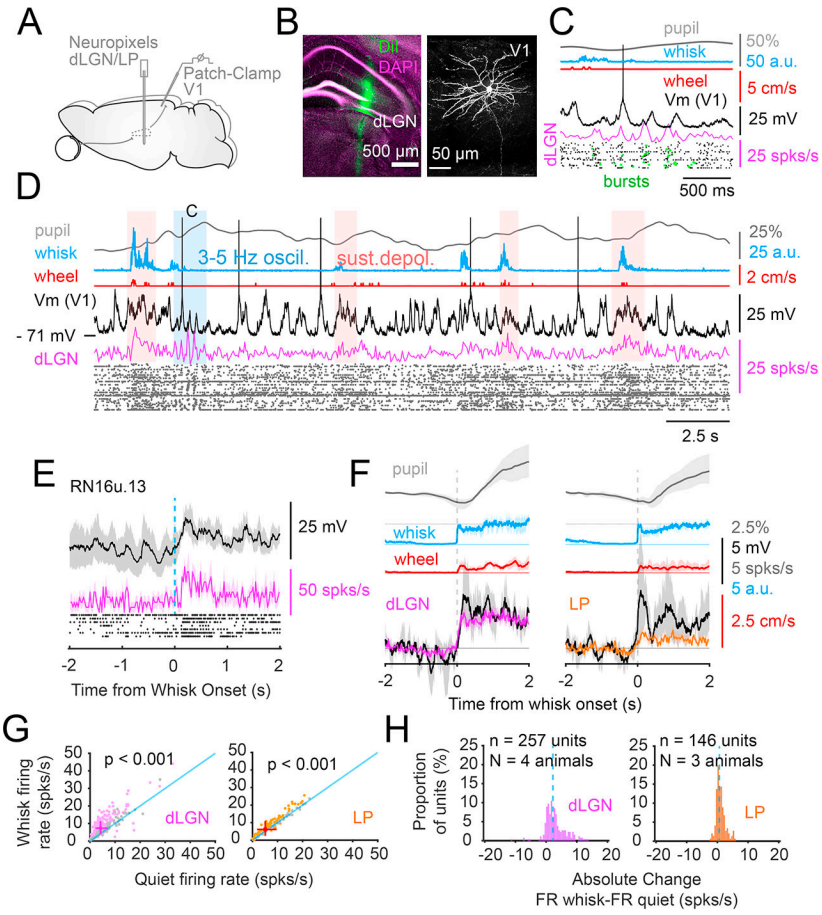


**Figure 2. Activity in the visual thalamus is synchronized to the onset of whisker movements and 3–5 Hz rhythmic oscillations.**

(A) Illustration of recording arrangement with a Neuropixels probe inserted into the dLGN and simultaneous whole cell recordings from V1 L2,3 neurons. (B) Illustration of the track of the Neuropixels probe (DiI labeling) through the dLGN and a biocytin fill of the simultaneously recorded layer 2/3 pyramidal neuron. (C) Example of the recording, illustrating the occurrence of a 3–5 Hz rhythm that is associated with the arrival of rhythmic PSP barrages in the cortical neuron and synchronized rhythmic discharge of dLGN neurons. Many of these discharges appear as action potential bursts (green dots). (D) Illustration of the recording on a longer time base. Note that when the animal whisks there is a sustained depolarization and increased dLGN activity. (E) Example of a dLGN unit activity (raster and average activity in purple) and V1 neuron membrane potential (black trace; cell in B,C,D) aligned to whisker movement onset. (F) Onset of the grand average of membrane potential change (n = 4 and 3 L2,3 neurons), dLGN (257 units), and LP (146 units) activity aligned to the onset of whisker movement (N = 4 and 3 animals). (G) Firing rate of dLGN and LP neurons during periods of whisker movement versus non-whisker movement. (H) Absolute change in activity in dLGN and LP neurons during periods of whisker movement versus non-whisker movement (bin size = 25 ms for dLGN and LP spike rates). Dashed blue lines indicate the median Shaded regions in graphs indicate 95% bootstrapped confidence interval. The crosses in scatter plots show the 25th and 75th percentiles with the center

representing the overall medians. The paired t-test (for normally distributed data), or the Wilcoxon signed rank sum test (non-parametric) were applied to test statistical significance in G. Units that were not significantly modulated by whisker movement are shown in grey.

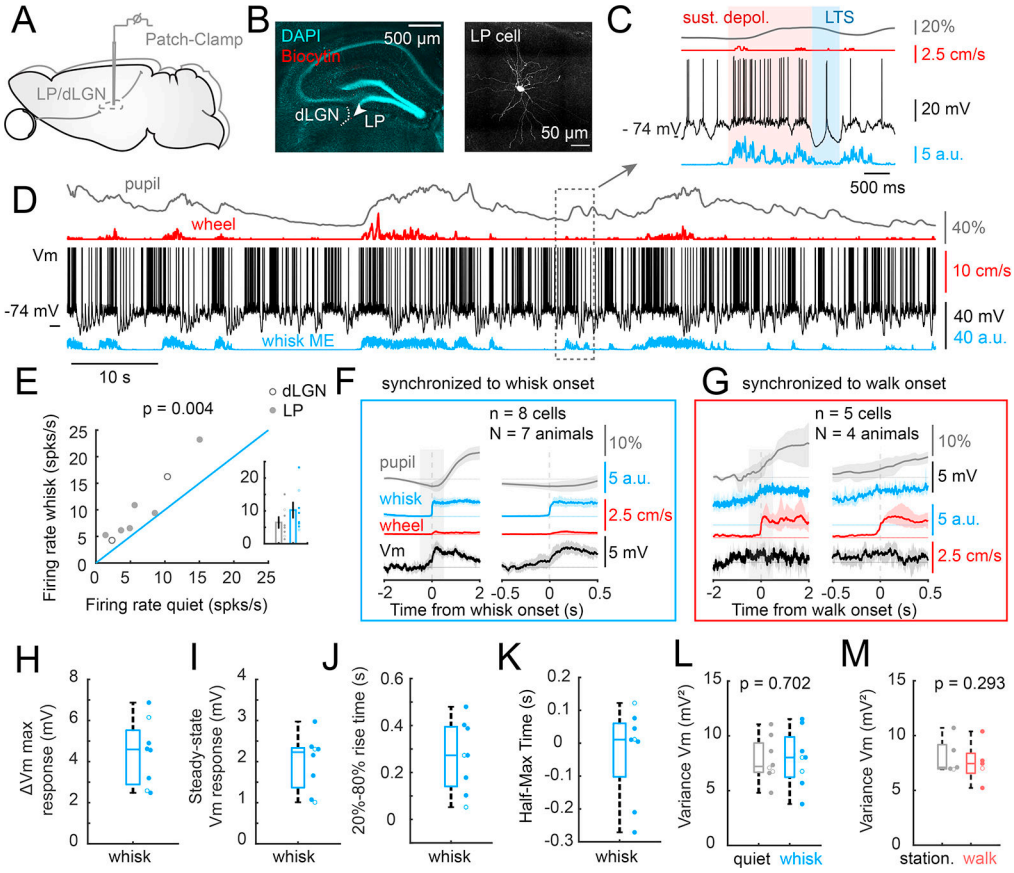


**Figure 3. Whole cell recordings from visual thalamic neurons reveal membrane potential dynamics associated with state changes and 3–5 Hz oscillations.**

(A) Illustration of whole cell recording from visual thalamus (dLGN/LP). (B) Histology illustrating the location of the recorded cell just inside the LP and biocytin recovery of morphology. (C) Detail of the recording shown in D. illustrating a depolarization of the membrane potential (black) associated with whisker movement (blue). A short 3–5 Hz oscillation with a low threshold $Ca^{2+}$ spike occurred upon reduction of whisker movement. (D) Longer time base illustrating the activity of the LP neuron shown in B. in relationship to pupil diameter, locomotion and whisker movement. Note the frequent sudden membrane potential hyperpolarizations that were often associated with 3–5 Hz oscillations. (E) The overall AP firing rate is significantly increased in the intracellularly recorded visual thalamic neurons during whisker movement. Alignment of the membrane potential to onset of whisker movement (F) demonstrates a rapid depolarization, while alignment with the onset of walking (G) does not. Two time bases are shown for clarity (F,G). Whisker movement-associated maximum changes in membrane potential (H), steady state depolarization (I), 20–80% rise time (J) and half max times (K) in visual thalamic neurons. The membrane potential variance does not significantly change with whisker movement, or locomotion (L,M). (n = 2 dLGN neurons (empty circles), n = 6 LP neurons (filled circles), N = 7 mice; no locomotion bouts occurred in 3 out of the 8 recordings). Shaded regions in graphs indicate 95% bootstrapped confidence interval. Boxplots show median, 25th and 75th percentiles and the whiskers indicate the most extreme data points that are not considered

outliers. Bar graphs in (E) indicate the mean and the error bars indicate the standard error of the mean. The paired t test (for normally distributed data), or the Wilcoxon signed rank-sum test (non-parametric) were applied to test statistical significance in (L) and (M). See also Figure S4.

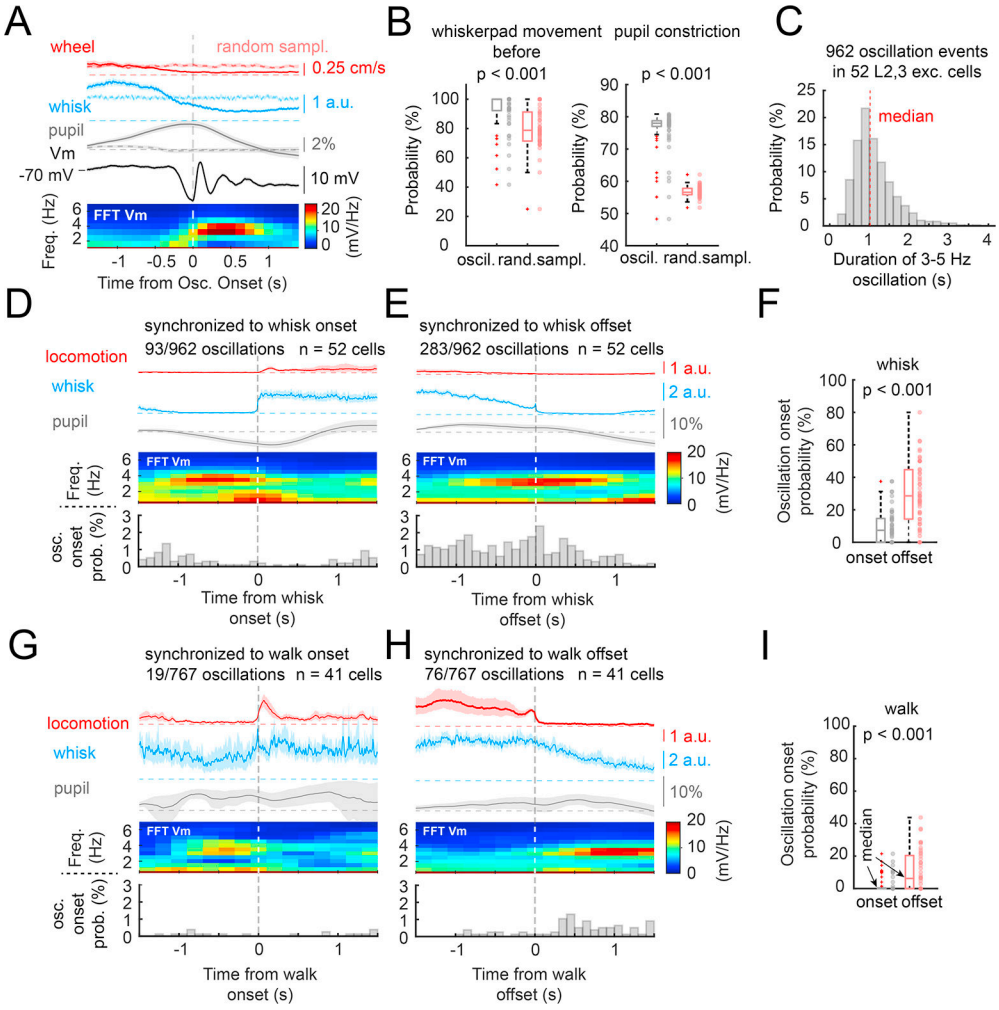


**Figure 4. 3–5 Hz Alpha-like oscillations preferentially occur during decreases in movement and arousal.**

(A) Alignment of averages in wheel movement, whisker pad movement, pupil diameter, and membrane potential FFT (fast Fourier transform) power density (1.25 s sliding window size, 90% overlap) to the onset of 3–5 Hz oscillations in the membrane potential of L2/3 neurons reveal that the onset of the oscillation is preceded by a decrease in locomotion and whisking, along with a dilation and constriction of the pupil diameter (n = 52 neurons, N = 41 animals). (B) Whisker pad movements (crossing a threshold of 0.5 a.u. during a time window of−2s until oscillation onset) and pupil constriction (time window = −0.5s until 0.5s) are associated with the oscillation at a significantly higher probability than in randomized data. (C) Distribution of the duration of 3–5 Hz oscillation events in cortical neurons. (D) and (E) Probability distribution of the onset of the 3–5 Hz oscillation, averaged membrane potential FFT power and averages of locomotion, whisker motion energy and pupil area relative to whisk onset versus offset. 93 out of 962 oscillations occurred within +/− 1.5 s of whisk onset (n = 52 cells), while 283 out of 962 oscillations occurred within +/− 1.5 s of whisk offset. Instances in which no oscillations occurred were not included for determining the averaged movement/pupil traces and the averaged FFT. (F) Probability by which the oscillations start within a window of − 1.5 s to + 1.5 s relative to whisk onset

versus offset. (G-I) Same as panels D-F, but for walk onset versus offset (n = 41 cells, N = 33 animals). Note that the general probability of a 3–5 Hz oscillation is low (D, G) and decreases dramatically just before and after the onset of whisking and walking. In contrast, decreases in whisking, or the cessation of whisking or walking, is associated with the increased occurrence of 3–5 Hz oscillations (E, H). Note that whisking typically precedes walking onset and tapers slowly following walking offset. Shaded regions in graphs indicate 95% bootstrapped confidence interval. Boxplots show median, 25th and 75th percentiles and the whiskers indicate the most extreme data points that are not considered outliers. The paired t test (for normally distributed data), or the Wilcoxon signed rank-sum test (non-parametric) were applied to test statistical significance in (B), (F) and (I).

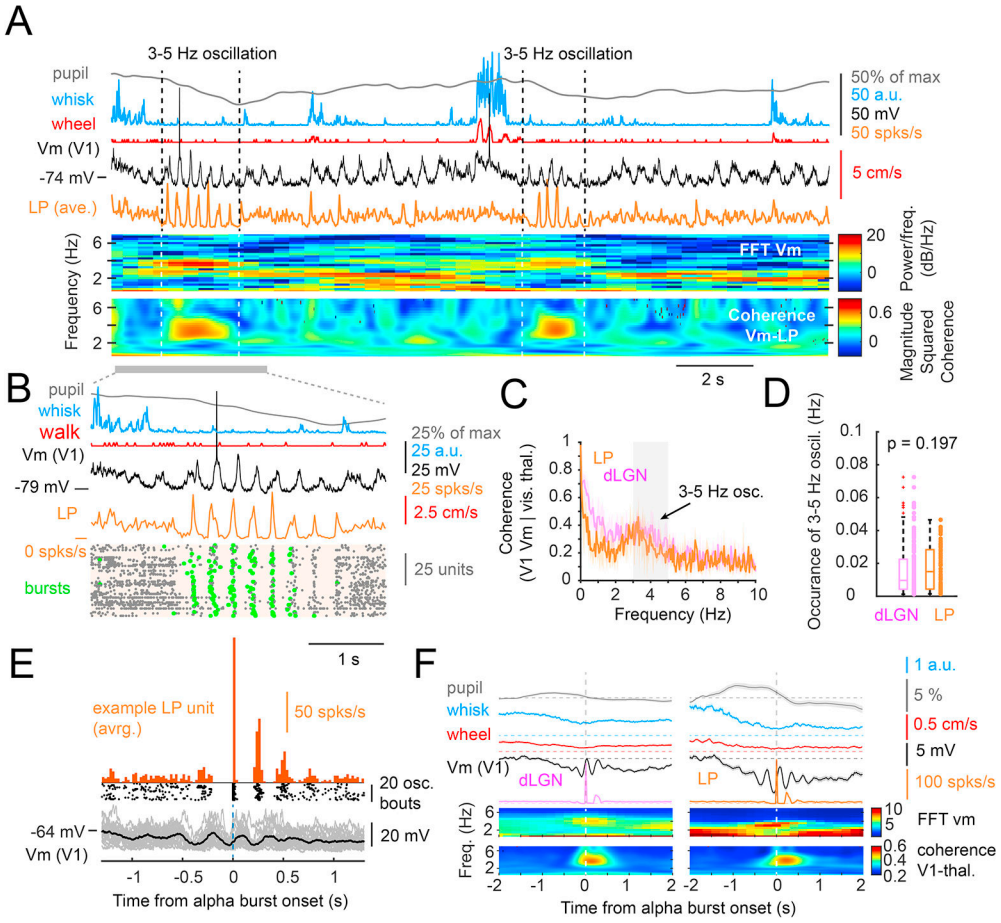


**Figure 5. Whole cell and Neuropixels extracellular recordings reveal 3–5 Hz oscillations to be highly synchronized between visual cortex and thalamus.**

(A) Simultaneous whole cell recording of a V1 neuron with Neuropixels recording of unit activity in the LP nucleus during example 3–5 Hz oscillations. The oscillation is associated with a sudden cessation of activity in LP neurons and a hyperpolarization of cortical neurons, followed by the arrival of rhythmic synaptic barrages and LP synchronized action potential discharge. FFT (4 s sliding window, 90% overlap) of the cortical L2/3 neuronal membrane potential reveals high power at 3–5 Hz during these oscillations and plots of coherence between the cortical membrane potential and the average firing rate of LP neurons reveals high thalamocortical coherence at these frequencies during the oscillations. (B) Expansion of one example 3–5 Hz oscillation illustrates the tight synchrony between cortical membrane potential oscillations and LP action potentials, many of which appear as bursts (green dots). (C) The membrane potential of V1 neurons and the summed action potential activity of visual thalamic neurons are highly coherent in the 3–5 Hz range (n = 7 L2/3 neurons, n = 403 dLGN/LP units, N = 7 animals). (D) The rate of occurrence of the 3–5 Hz oscillation is similar in the dLGN and LP (for dLGN: n = 176 units (out of 257; 81 units did not exhibit 3–5 Hz oscillation AP bursts), N = 4 animals; for LP: n = 91 units (out of 146), N = 3 animals). (E) Illustration of the averaged membrane potential of a V1 neuron synchronized to the onset of 3–5 Hz oscillation bouts in an example LP unit. (F) Alignment of grand average of whisker movement, walking, pupil diameter, and L2,3

V1 Vm, membrane potential FFT power, and thalamic action potential rate coherence, with onset of 3–5 Hz oscillations in dLGN and LP (bin size = 25 ms for dLGN and LP spike rates). Shaded regions in graphs indicate 95% bootstrapped confidence interval. Boxplots show median, 25th and 75th percentiles and the whiskers indicate the most extreme data points that are not considered outliers. The Wilcoxon rank-sum test was applied to test statistical significance in (D).

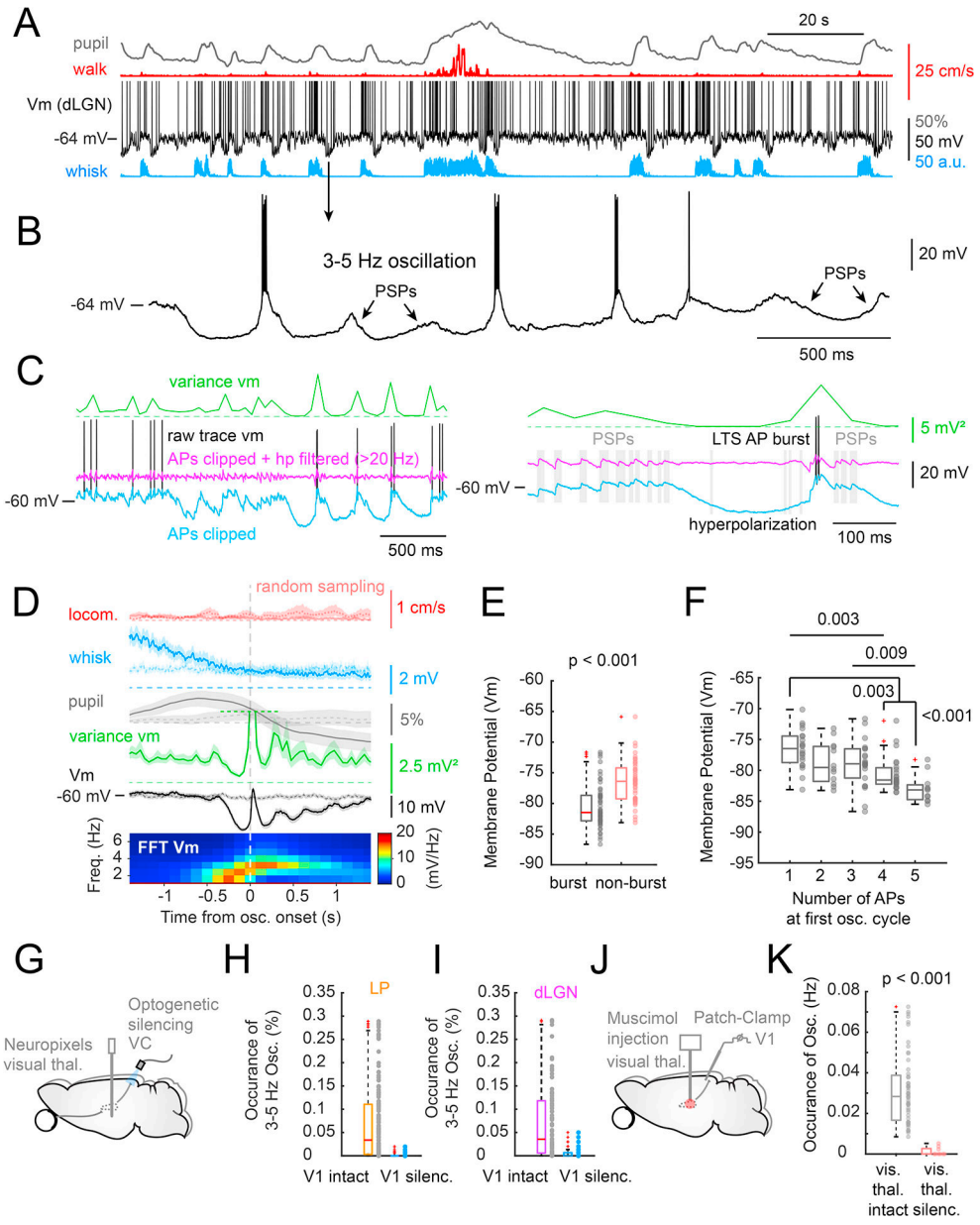


**Figure 6. Alpha oscillation appears as a sequence of hyperpolarizing and depolarizing events that trigger low threshold $Ca^{2+}$ spikes in thalamic neurons.**

(A) Intracellular recording in a dLGN thalamocortical cell revealing frequent bouts of 3–5 Hz alpha oscillation. Note that in this cell these often occur after a whisker movement bout. (B) Expansion of one of these oscillations revealing a sequence initiated by a deep hyperpolarization associated with a relatively smooth membrane potential, followed by the generation of a low threshold $Ca^{2+}$ spike that initiates several action potentials. The next two cycles of the oscillation appear as PSP barrages, with the next two cycles initiating low threshold $Ca^{2+}$ spike mediated bursts. The final cycles of the oscillation illustrated appear as PSP barrages. (C) Examination of membrane potential variance preceding and during a 3–5 Hz oscillation reveals the variance to be near zero during the hyperpolarizing phases of the oscillation, suggesting that it is mediated by the withdrawal of synaptic

activity. Black trace = raw recording; blue trace = APs removed from raw trace; pink trace = APs removed and raw trace high pass filtered (>20 Hz); green trace = variance of membrane potential calculated from the pink trace (bin size = 50 ms). (D) Illustration of the timing of whisking, walking, pupil diameter, vis. thalamic Vm variance, Vm, and FFT power of the membrane potential synchronized to the onset of the 3–5 Hz oscillation (99 oscillations in n = 8 neurons; N = 7 animals). Note the marked decrease in whisking and pupil diameter associated with the onset of the rhythm, and the large alterations in membrane potential variance during the oscillation. (E) The membrane potential preceding the occurrence of a low threshold $Ca^{2+}$ spike mediated burst was significantly more negative than when a burst did not occur. (F) The hyperpolarized level of the membrane potential prior to the onset of each low threshold $Ca^{2+}$ spike correlated with the number of action potentials generated during the first cycle of the oscillation. (G) Illustration of visual cortical optogenetic silencing experiment. (H, I) Silencing visual cortex resulted in a nearly complete abolition of the occurrence of 3–5 Hz oscillations in both the LP (H) and dLGN (I) (LP, n =149 units, N = 4 animals; dLGN, n = 85 units, N = 2 animals). (J) Illustration of thalamic silencing through muscimol injection. (K) Silencing of visual thalamus results in a near complete abolition of 3–5 Hz oscillations in L2,3 V1 neurons (control neurons same as Fig.4A, n = 52 neurons. N = 41 animals; silenced group n = 9 neurons, N = 5 animals) Shaded regions in graphs indicate 95% bootstrapped confidence interval. Boxplots show median, 25th and 75th percentiles and the whiskers indicate the most extreme data points that are not considered outliers. The paired t-test (for normally distributed data), or the Wilcoxon signed rank sum test (non-parametric) were applied to test statistical significance in H and I. The Kruskal Wallis test with posthoc Bonferroni correction was used for data shown in F. The unpaired t-test (for normally distributed data), or the Wilcoxon rank sum test (non-parametric) were applied to test significance in E and K. See also Figures S4 and S5.

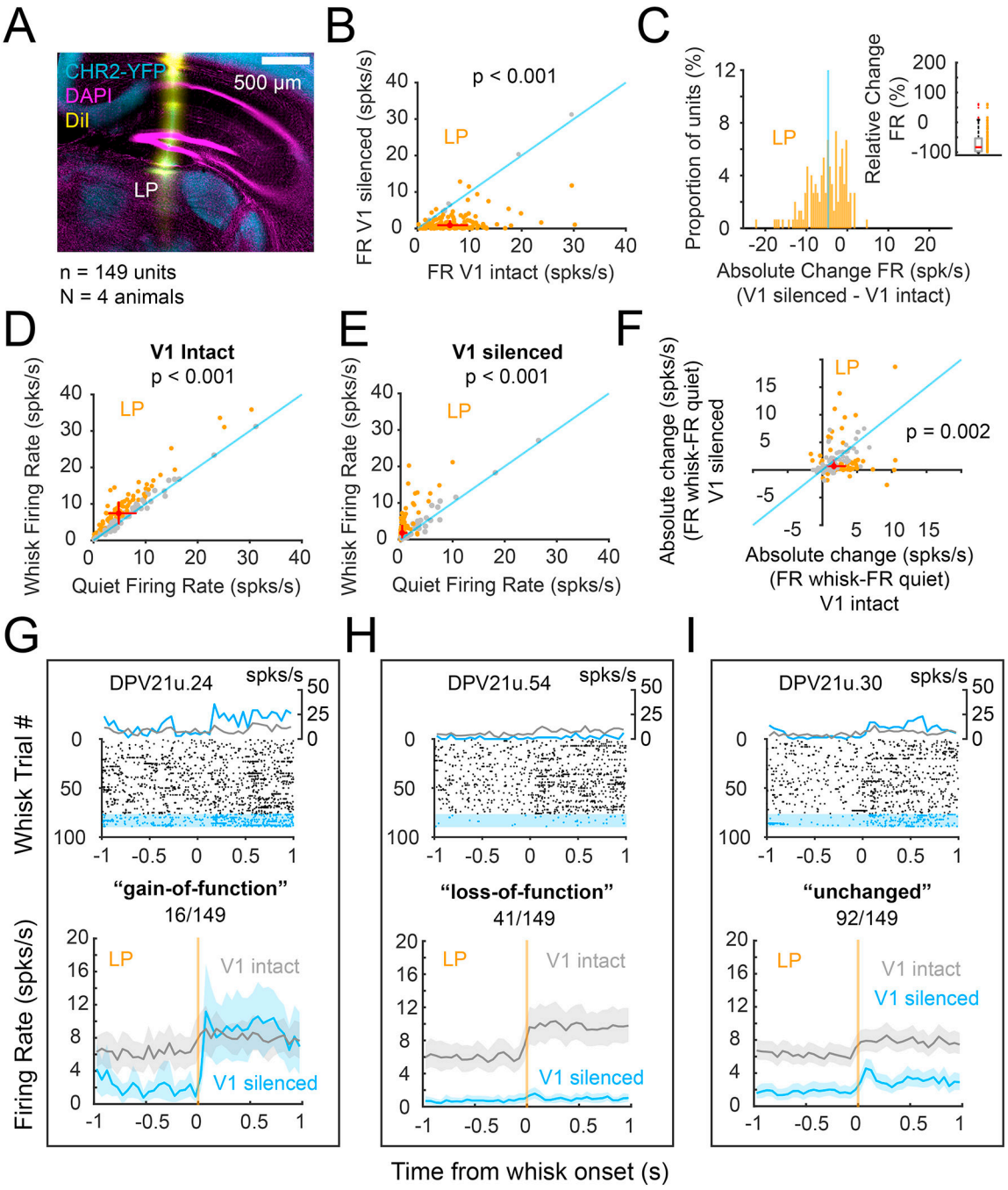


**Figure 7. Effects of movement on LP thalamic activity with and without silencing of visual cortex.**

(A) Illustration of the Neuropixels electrode track through the LP nucleus. (B) Silencing of the visual cortex dramatically reduces activity in many LP neurons. (C) Absolute change in firing rate of LP neurons with V1 silencing. (D) and (E) whisker movement significantly increases the firing rate of LP neurons in either normal (D) or visual-cortical silenced (E) conditions. Orange dots represent cells with a significant change in activity with whisker movement vs. quiescence. (F) Distribution of whisker movement induced change in LP firing rate with and without visual cortical silencing (orange dots represent

units with statistically significant difference between V1 intact and silent). Examples and group averages of LP cells that increased their whisker movement-associated firing rate changes (G), decreased (H) or showed no significant change (I) with silencing of V1 (bin size for spike rates = 50 ms). The paired t-test (for normally distributed data), or the Wilcoxon signed rank sum test (non-parametric) were applied to test statistical significance in D-F. The crosses in scatter plots show the 25th and 75th percentiles with the center representing the overall medians. Data points in F represent the average of bootstrapped means. Statistical significance for each of the data points in F was assessed by testing whether the bootstrapped 95% confidence intervals (not shown) crossed the reference line (shown in blue). Shaded regions in G-I indicate 95% bootstrapped confidence interval. See also Figures S5 and S6.

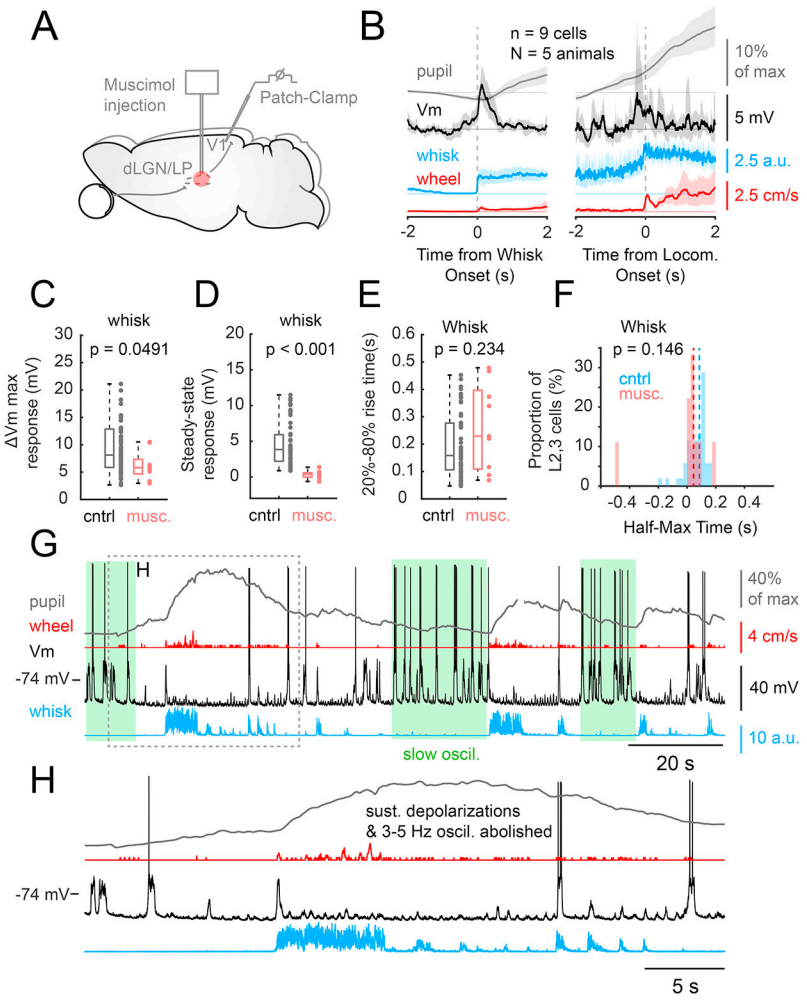


**Figure 8. Effects of silencing of visual thalamus on movement related activity in V1.**

(A) Illustration of experimental situation. The visual thalamus was silenced with microinjection of the $GABA_A$ agonist muscimol. Following injection, whole cell recordings were performed in V1 of awake mice. (B) Alignment of visual cortical neuronal membrane potential with the onset of whisker pad movement or of locomotion revealed transient depolarizations that were not sustained. The depolarization was more highly synchronized with the onset of whisker pad movement than locomotion. The change in membrane potential in cells recorded during silencing of activity in the visual thalamus (n = 9 cells in N = 5 mice) contained a transient component that was significantly smaller than in control cells (controls = same data as shown in Fig. S2) (C), and which exhibited a greatly reduced sustained component during whisker movement (D). (E) The 20%−80% rise time of the transient depolarization was not affected by inhibition of the visual thalamus. (F) Distribution of half-maximum time for control and thalamic-inhibited cells. (G) Example of whole cell recording of a representative L2,3 V1 neuron in the waking mouse following inhibition of the visual thalamus. Note the lack of sustained depolarizations, particularly during bouts of whisker pad movement. (H) Expansion of a portion of the recording in G illustrating the transient nature of synaptic barrages during whisker and wheel movement. Shaded regions in graphs indicate 95% bootstrapped confidence interval. Boxplots show

median, 25th and 75th percentiles and the whiskers indicate the most extreme data points that are not considered outliers. The unpaired t-test (for normally distributed data), or the Wilcoxon rank sum test (non-parametric) were applied to test significance in C-F. See also Figure S7.

## KEY RESOURCES TABLE

| REAGENT or RESOURCE | SOURCE | IDENTIFIER |
|---|---|---|
| Chemicals, peptides, and recombinant proteins | | |
| Biocytin | Sigma | Cat#B4261 CAS 40709–69–1 |
| Streptavidin, alexa fluor 555 | Thermo Fisher Scientific | Cat# S32355; RRID AB_2571525 |
| DAPI | Sigma | Cat# D9542 CAS 28718–90–3 |
| Muscimol, BODIPY™ TMR-X Conjugate | Thermo Fisher Scientific | Cat# M23400 |
| Vybrant™ DiI Cell-Labeling Solution | Thermo Fisher Scientific | Cat# V22885 |
| Experimental models: Organisms/strains | | |
| Mouse: Ai32 | The Jackson Laboratory | B6.Cg-Gt(ROSA)26Sor$^{tm32(CAG-COP4*H134R/EYFP)Hze}$/J |
| Mouse: C57BL/6J | The Jackson Laboratory | 000664 stock number |
| Mouse PV-cre | The Jackson Laboratory | B6.129P2-Pvalb$^{tm1(cre)Arbr}$/J |
| Software and algorithms | | |
| DeepLabCut | Mathis et al., 2018 | https://github.com/DeepLabCut/DeepLabCut |
| FaceMap | Stringer et al., 2019 | https://github.com/MouseLand/facemap |
| ImageJ | National Institute of Health | RRID:SCR_003070 |
| Kilosort2 | Pachitariu et al. 2016 | https://github.com/MouseLand/Kilosort |
| LabView 2016 | National Instruments | RRID:SCR_014325 |
| Matlab 2016b and 2019b | MathWorks | RRID:SCR_001622 |
| Phy2 | Rossant et al., 2016 | https://github.com/cortex-lab/phy |
| Other | | |
| Matlab analysis code with example recordings | This study | https://doi.org/10.5281/zenodo.5539784 |